PREPARATION AND CHARACTERIZATION OF SPIN-COATED COLLOIDAL TEMPLATES AND PATTERNED ELECTRODEPOSITED COBALT

KITTY KUMAR

PREPARATION AND CHARACTERIZATION OF SPIN-COATED COLLOIDAL TEMPLATES AND PATTERNED ELECTRODEPOSITED COBALT

by

© Kitty Kumar

A thesis submitted to the
School of Graduate Studies
in partial fulfillment of the
requirements for the degree of
Master of Science.

Department of Physics and Physical Oceanography
Memorial University of Newfoundland

December 19, 2008

St. John's Newfoundland

Contents

Abstract

Patterned magnetic materials are potential candidates for magnetic data storage. Many different techniques have been proposed to fabricate such materials, but the high costs involved have limited their commercial viability. We propose a fast and cheap method of fabricating patterned magnetic materials by electrodepositing through spin coated silica colloidal templates.

The structure of the templates prepared by spin coating was analyzed by using scanning electron microscopy, laser diffraction and atomic force microscopy. The structure, thickness, and symmetry present in the templates depends on the spin speed and type of solvent used in making the colloidal suspension for spin coating. We found that the templates are unique orientationally correlated polycrystals, exhibiting short-range positional order and long-range radial orientational correlations [C. Arcos, K. Kumar, W. González-Viñas, R. Sirera, K.M. Poduska and A.Yethiraj. *Physical Review E*, 77:050402/1-4, 2008.].

Based on these templates, a method for preparing patterned cobalt electrodeposits was devised. Scanning electron microscopy (SEM) studies showed that electrodeposition produces a cobalt anti-dot array, which conserves the four or six-fold symmetry present in the template. A method for calculating the lateral periodicity and thickness uniformity of the sample by SEM and atomic force microscopy (AFM) was devised.

Acknowledgements

I would like to express my sincere appreciation and gratitude to my supervisors Dr. Anand Yethiraj and Dr. Kris Poduska for their support, guidance, and helpful discussions. I am also grateful to Dr. Yethiraj for teaching me to handle a variety of experimental techniques. His devotion to the field of colloidal science has stimulated me a lot in the long path towards being an experimental physicist. I am grateful to Dr. Poduska for our helpful discussions about electrochemistry and for teaching me sample preparation, and atomic force microscopy. I thank Dr. Clouter and Ms. Lisa Lee for their respective help with vacuum evaporation and scanning electron microscopy. I am thankful to my instructors, Dr. S. Curnoe and Dr. K. Nag for their help with the successful completion of my coursework. Thank to Dr. González-Viñas for laser diffraction data analysis. I am thankful to Dr. Arcos for beginning this project and for her cooperation. I am also appreciative of the support I received from my friend Bhuwan Sood.

I wish to thank my parents, my sister and brother for their support and guidance. I dedicate this thesis to them.

List of Tables

List of Figures

Chapter 1

INTRODUCTION

In this chapter, we will introduce colloidal self-assembly and its use as a templating technique for the production of a patterned array of a material. We will discuss the importance of studying magnetic patterned arrays and the techniques being used to prepare them. After discussing our choice of cobalt as a system to study, an overview of the thesis is given.

1.1 COLLOIDS

The name *colloid* was given to "glue-like" materials by Thomas Graham in 1861.[1] The colloids came to his attention while studying the process of osmosis, *i.e.* the diffusion of particles from a solution to a pure solvent through a membrane. Depending on the number of constituent atoms or molecules, the colloidal regime extends between the length scales of tens of nanometers to a few micrometers.

Generally, colloidal particles are dispersed in a fluid medium to form colloidal dispersions. One unknowingly deals with many colloidal dispersions in daily life, such as milk, paint, ink, *etc.* In a colloidal dispersion, particles undergo random motion called Brownian motion, which is due to their thermal motion and collisions with the comparatively small-sized particles of the fluid medium. The colloids also possess unique properties of crystallizing in a particular crystal structure and showing phase transitions like a molecular system. Different interaction forces (such as the electrostatic force and the effective force due to excluded volume) contribute to the formation of colloidal crystal structures, which are analogous to those in molecular systems.

1.2 SELF-ASSEMBLY IN COLLOIDS

Colloids have fascinating properties, both as the model systems to probe fundamental phenomena (such as phase transitions, crystallization, melting, *etc.*) in condensed matter physics, and as templates for patterned materials with diverse applications. Micron-sized colloidal particles have gained special attention because of their typical length scales ($\sim$ microns) and time scales ($\sim$ seconds), which are measurable by experimental techniques. Thus, their structure and dynamics can be studied on a single particle level. Moreover, colloidal crystals are of potential importance in materials science. Colloids can self-assemble

in periodic arrays and can form colloidal crystals. Opals are gem stones that are an example of naturally occurring colloidal crystals. Natural opals consist of randomly close-packed 150-500 nm diameter colorless silica particles.[2] Because the three-dimensional array formed by the silica particles has a lattice constant comparable to the wavelength of visible light, these natural opals show a beautiful iridescence called opalescence. The structure consists of high refractive index silica spheres ($n \approx 1.5$) filled with air having a lower refractive index ($n = 1$). The periodic modulation of the refractive index contrast between the silica particles and the air results in the phenomenon of opalescence. Figure 1.1 shows the opalescence in a colloidal crystal prepared by the dip-coating technique in our laboratory. The ability of

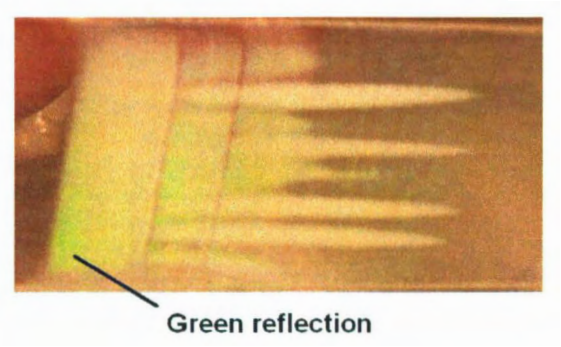

Figure 1.1: A colloidal crystal prepared by the dip-coating technique in our laboratory. The green color is due to Bragg reflections from a close-packed colloidal crystal.

colloidal spheres to self-organize into crystalline structures with a visible optical length scale has motivated researchers to synthesize opals and tailor their properties for the fabrication of devices such as optical sensors,[3] thermophotovoltaics,[4–6] filters[7] and photonic band gap structures.[8]

1.3 SPIN COATING: METHOD TO ASSEMBLE COLLOIDAL SPHERES

Much work is being done by researchers to crystallize colloids in different crystal structures with the help of external forces like shear,[9,10] gravitational,[11] electric and electrohydrodynamic fields.[12-14] Making dried colloidal crystals with these methods is slow, taking from hours to days. In all methods, the colloidal spheres are allowed to diffuse slowly to attain a stable low-energy configuration. As the solvent evaporates from the colloidal suspension, the spheres come together due to capillary forces and form a close-packed structure on a substrate. With these slow preparation techniques, one can prepare colloidal crystals of dimensions 10-100 μm^2. Like natural opals, the dried colloidal crystals prepared by the aforementioned methods contain a large number of defects. These defects can arise because of polydispersity in the colloidal particle diameters, or polycrystalline domains or vacancies (point defects) in the crystal.

The technique of spin coating has been used for decades to deposit photoresists,[15] protective coatings[16] and anti-reflective coatings on optical components.[17] It can also be used to produce three-dimensional colloidal crystals.[18,19] Spin coating is the quickest and most reproducible method to produce colloidal assemblies. It has been shown to be a robust technique,[18-20] making large-area colloidal crystals in minutes. The ability to control the film thickness by tuning spin speed and spin time, and to produce monolayers, are other advantages over other techniques such as dip-coating. Even though a lot of work has been done in this field, the true structure of spin coated colloidal coatings was still not well known. The work in this thesis has contributed toward this understanding.[21] The structure of a colloidal coating prepared by Jiang *et al.*[18] was analyzed by scanning electron microscopy (the top surface of the crystal only, and far from the center of spinning) and normal incidence VIS-IR spectroscopy. The colloidal crystals were prepared by spin coating a suspension of colloidal

particles in a less volatile medium, consisting of a monomer. The spin coated particles were arranged in hexagonal layers, such that the particles in the bottom layers touched the layers above. On the other hand, particles within a single hexagonal layer did not touch each other. Mihi *et al.*[19] used reflection spectroscopy at normal incidence to study the lattice constant of spin coated colloidal crystals. All structure analyses were done over small regions and thus did not reflect the overall structure of a spin coated colloidal film. In this thesis, we used scanning electron microscopy, laser diffraction and atomic force microscopy to correlate the local structure of spin coated colloidal films on a larger scale.[21]

1.4 TEMPLATED MAGNETIC MATERIALS: SYNTHESIS AND IMPORTANCE

The technology of magnetic data storage has developed rapidly in the last 50 years, with scientists trying to achieve higher areal density and aiming for the higher efficiency, speed and compactness. Further increases of areal density in a conventional thin film media faces limitation due to thermal instability caused by demagnetizing fields at the transition boundary and noise caused by collective magnetization. This has led to the idea of patterned magnetic media in which demagnetization effects and noise are lowered by bit separation.[22,23] Various lithographic techniques, such as e-beam lithography, X-ray lithography, nano-imprint lithography and interference lithography, have been developed in the last 20 years for the production of such magnetic media,[24] but higher costs have limited their commercialization. Template-guided electrodeposition of magnetic materials provides an opportunity to reduce the cost and scale of periodicity in the deposited magnetic structures to increase the areal density over large areas, which is not achievable by lithographic techniques.[23] Self-assembly of magnetic particles themselves on a substrate is an alternative approach to prepare high

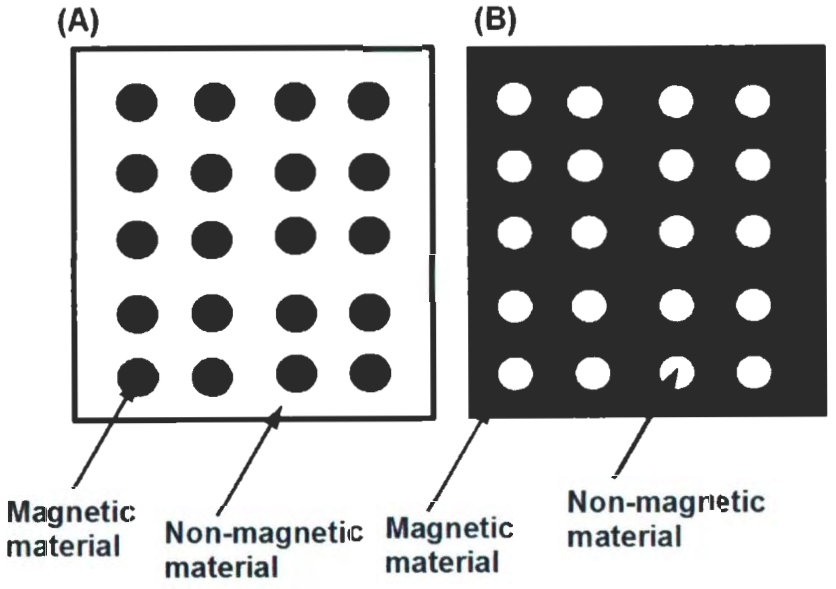

Figure 1.2: Two types of magnetic arrays. (A) A dot-array consists of isolated magnetic structures (dots, wires, cylinders, *etc.* depicted in black) separated by a non-magnetic material. (B) An anti-dot array consists of a thin film of the magnetic material (depicted in black) interspersed with non-magnetic regions (white).

density magnetic media.[25]

The process of electrodeposition or electrochemical deposition was first used after 1840 with the development of electrolytes for silver and gold deposition. Today, electrodeposition has made itself compatible with different fields, contributing towards fast and efficient technology. The ability to deposit material into three-dimensional geometries with thickness ranging from a millimeter to a sub-micron scale is one great strength of electrodeposition. Unlike physical vapor deposition techniques, electrodeposition provides an advantage of depositing materials over partially-shielded surfaces. Magnetic arrays are potential can-

didates for a high density information storage media. These arrays can be divided into two categories, *i.e.* dot and anti-dot arrays. The first category, dot-arrays, consist of isolated magnetic structures (dots, wires, cylinders, *etc.*) separated by a non-magnetic material (Figure 1.2A). Alternatively, anti-dot arrays consist of a thin film of magnetic material interrupted by non-magnetic regions (Figure 1.2B). Either dot or anti-dot arrays can be prepared by electrodeposition, depending on the type of template used. People have examined magnetic arrays prepared by electrodeposition through various kinds of templates, such as nanochannel alumina,[26] track-etched membranes,[27] spin coated block co-polymers[28] and self-assembled colloidal crystals.[29 32] Though lack of long-range order has limited the use of the self-assembled colloidal crystals as templates, the advantage of controlling the shape and size of electrodeposited magnetic structures has drawn the attention of researchers toward this technique.[29 33]

Spin coating is one technique that can be used to guide colloidal crystals; it assembles colloids into crystals in a unique way.[21] Much work is being done on spin coating colloids, including the idea of using them as templates for electrodeposition of magnetic materials.[29 33] This thesis work is based on using these uniquely ordered colloidal crystals as templates for electrodepositing cobalt and characterizing the template structure, toward the eventual goal of producing electrodeposited magnetic anti-dot arrays.

1.5 WHY ARRAYS OF COBALT?

Magnetic information is stored in the form of bits in the two states of magnetization of a magnet ("up" and "down"). In dot or anti-dot arrays, the magnetization reversal of each bit is modified by the presence of non-magnetic regions. The spins that are surrounded by non-magnetic regions are typically more difficult to reverse. To gain even more stability against spontaneous flipping due to thermal energy, one needs a storage medium with high

shape anisotropy and high crystalline anisotropy.[22,23] Cobalt possesses high crystalline and shape anisotropy compared with other ferromagnetic materials, such as iron and nickel. It forms a hexagonal crystal structure, with only the hexagonal axis being the easy axis.[34] The domains of cobalt are needle like, the high axial ratio (c/a) results in high shape anisotropy of the cobalt.[35] Because of the high shape and crystalline anisotropy, cobalt is a preferred material for magnetic storage media.

1.6 SCOPE OF THIS THESIS

In this thesis work, we used the spin coating method to prepare colloidal silica templates. Cobalt was electrodeposited through the prepared templates to get a patterned array. Chapter 2 describes the techniques used for preparation and characterization of our samples. These preparation techniques (spin coating and electrodeposition) are discussed in terms of their challenges. This is followed by descriptions of template and electrodeposit characterization techniques, including scanning electron microscopy, atomic force microscopy and laser diffraction.

Chapter 3 describes the step-by-step preparation of a cobalt anti-dot array. The process is initiated by making a colloidal suspension, preparing substrates, and spin coating to make a template (whose unique structure is described in Chapter 4). The design and cleaning of substrates to prepare them for electrodeposition is also described in Chapter 3, including details of the electrodeposition procedure. The complications and results of electrodepositing cobalt under different conditions are also summarized. To get an anti-dot array, one needs to etch colloids with hydrofluoric acid. The procedure and results of etching the prepared samples, and related issues, are mentioned at the end of Chapter 3.

Chapter 4 deals with the characterization of the templates and electrodeposited samples. The structure of a spin coated colloidal template (at different speeds) by spin coating a

suspension (prepared in different solvents) is described in terms of thickness variation studies at different speeds. The procedure for determining lateral periodicity and uniformity of patterned cobalt samples by atomic force microscopy and scanning electron microscopy is also described in this Chapter. The conclusions drawn from the work are summed up in Chapter 5.

Chapter 2

EXPERIMENTAL AND CHARACTERIZATION TECHNIQUES

2.1 SPIN COATING

Spin coating involves spreading a liquid or a suspension dispensed onto the center of a rotating substrate. The liquid is dispensed by a pipette onto a substrate rotating at a constant angular speed. The spinning speed of the substrate is generally controlled to get a film with the desired thickness, as thin as nanometer-scales. The viscosity and volatility of a solvent,[36] the amount of solid content in the suspension,[37] spinning time and surface tension are additional factors that affect the thickness of a spin coated film.[19] As the substrate rotates, the net viscosity of the suspension increases due to evaporation until the liquid no longer spreads. Spin coating involves the competition between various forces, such as centrifugal force, viscous force and the evaporation rate of the solvent.[38] In order to get a thinner film, one should spin coat a suspension in a low-viscosity solvent and/or non-volatile

solvent at a high spin coating speed.

For a non-volatile solvent, the thickness (h) of the colloidal film is proportional to the power N of the angular speed (ω). The spin time (T) also inversely affects the thickness of the deposit (Equation 2.1).[39]

$$h \propto \frac{\omega^{N}}{T} \tag{2.1}$$

For a given volatile solvent and a spin speed, T has a definite value and is not a convenient control parameter. Thus, for volatile solvents like acetone and ethanol, we can approximate Equation 2.1 by

$$h \propto \omega^{N'}, \tag{2.2}$$

where we absorb any possible dependence of T on ω into the power law as done previously by Mihi *et al.*[19] The value of N' depends on the amount of solute present in the suspension. Rehg *et al.*[37] varied the ionic strength by varying the salt concentrations in the suspension and found that the value of N' ranges from 0.44 - 0.51 for salt concentrations ranging from 0.0 - 0.1 M. The thickness of the coating is also affected by the factors such as temperature and humidity, as these factors affect the rate of evaporation of the solvent.[40] The vapor of the evaporated solvent can also affect the rate of evaporation in a closed lid spin coater.

In our experiments, we spin coat colloidal suspension from volatile solvents (acetone or ethanol) on Au/Cr/glass substrates using a Laurell Technologies WS-400 spin coater (speed limit: 0 - 8000 rpm). For all of our spin coating experiments, we set the acceleration at 1710 rpm/sec, and we let the spinning reached the target speed before coating, so the acceleration was not variable. Our suspensions contain 20% silica spheres relative to the total volume of the suspension. During spin coating, the volatile solvent evaporates in seconds and leaves colloidal particles arranged in a particular structure, with voids available for the filling of a material.

2.2 ELECTRODEPOSITION

Electrodeposition is a well established technique that has been used for decades. Various books discuss the basic process.[41,42] Electrodeposition involves deposition of a material onto a conducting substrate by the application of a voltage. The type of material deposited during electrodeposition depends on the applied potential and the electrolyte content. Our electrodeposition experiments are done in a three electrode cell containing a working electrode, counter electrode and reference electrode. The electrodes are dipped in an aqueous solution of a metal salt (electrolyte). A potentiostat is used to maintain a constant (specified) potential at the working electrode with respect to the reference electrode. All potentials in this thesis are reported with respect to a standard Ag/AgCl (saturated KCl) reference electrode. The working electrode is the one on which the material is deposited, and complementary chemical reactions occur at the counter electrode. For example, electrodeposition of cobalt metal from a $CoSO_4$ (cobalt sulphate) electrolyte involves the following reactions:[43]

Counter electrode (Oxygen evolution)

$$2H_2O \rightarrow O_2 + 4H^+ + 4e^- \tag{2.3}$$

Working electrode (Cobalt ion reduction and hydrogen evolution)

$$Co^{2+} + 2e^- \rightarrow Co \tag{2.4}$$

$$2H^+ + 2e^- \rightarrow H_2 \tag{2.5}$$

The Nernst potential defines the equilibrium potential at which the desired reaction takes place. For example, the Nernst potential for cobalt deposition in our electrolyte is 0.65 V *vs.* Ag/AgCl, and in our experiments, a voltage of -1.2 V *vs.* Ag/AgCl is used to deposit cobalt. At this potential, H_2 gas is also evolved at the working electrode (Equation 2.5) and O_2 is evolved at the counter electrode (Equation 2.3). During these electrochemical reactions, the

bulk pH of the electrolyte could change due to production of the acidic/basic species. To stabilize the pH of the electrolyte, a buffer can be used. In our experiments, H_3BO_3 (boric acid) was used as a weak buffer to stabilize the electrolyte's pH.

One can estimate the thickness of the deposited metal by calculating the charge passed during deposition and the area of the substrate used for deposition. For simplicity, we assume that all the charge passed is related to cobalt deposition (Equation 2.4). The average thickness of the deposit (T) can be estimated by using Equation 2.6.[44]

$$T = \frac{M}{nFAD} \int Idt = \frac{Mq}{nFAD}, \tag{2.6}$$

where F = Faraday's constant (9.6×10^4 C/mol),

A = area of the deposit,

D = density of metal deposited (for cobalt, $D = 8.9$ g/cm^3),

M = molecular weight of metal (for cobalt, $M = 58.9$ g/mol),

q = total charge passed through the system during deposition,

I = current passed for small time dt,

n = charge on metal ion (for cobalt, $n = 2$).

In reality, a significant portion of the charge (10-60%) will be related to hydrogen evolution (Equation 2.5). Thus, the above would give an upper limit on thickness. However, note that the above has assumed $D = 8.9$ g/cm^3 for cobalt (*i.e.* a 100% dense deposit with no gaps or pores). If the material has is not dense, the thickness would be more than the estimated thickness.

Unlike other techniques (*e.g.* vacuum evaporation), electrodeposition starts at the metal surface (substrate) and the electrodeposit can grow around obstacles. Electrodeposition even fills masked spaces (as shown in Figure 2.1A) and after etching the template, patterned material will be left. Techniques like vacuum evaporation require a line-of-sight path to the substrate. Thus, etching the template shown in Figure 2.1B will remove the deposited

material with the template.

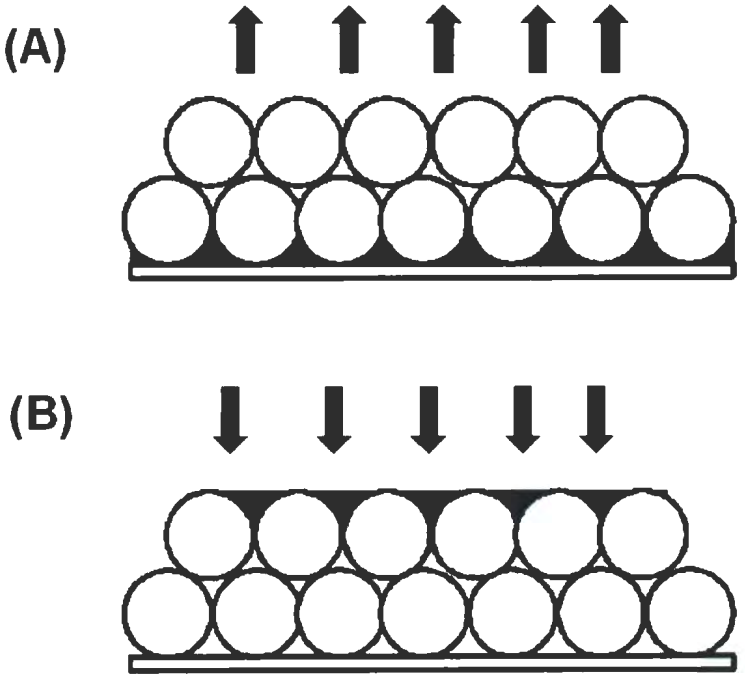

Figure 2.1: (A) Electrodeposition allows growth around obstacles, whereas (B) shows material deposition on the template by vacuum evaporation, in the absence of a line-of-sight path to the substrate.

2.3 SCANNING ELECTRON MICROSCOPY

Scanning electron microscopy (SEM, performed with a Hitachi S-570 in the Department of Biology) was used to image colloidal templates and templated cobalt samples after etching. SEM has been used for decades, and its fundamentals and details can be found in many books.[45,46] It is a tool that uses a high energy electron beam (few hundreds of eV to tens of keV) to image the surface of a solid sample. This instrument provides limited information about the height variations along the sample. Higher magnification and high resolution of scanning electron microscopy makes it more efficient and useful than a simple optical microscope. The focused electron beam interacts with the atoms present in the sample to produce both X-rays and elastically backscattered electrons. The intensity of the backscattered electrons is directly proportional to the atomic number (Z) of the material: the higher the atomic number of the element, the higher the intensity. Thus, for our samples, we expect to get a higher intensity from cobalt compared to silica. However, intensity also depends on the height differences. Samples need to be highly conducting for good SEM images to prevent charging effects. A sample can be coated with a thin layer of gold or carbon prior to imaging, or can be glued using silver paste, to provide a better conduction path.

2.4 ATOMIC FORCE MICROSCOPY

Atomic force microscopy (AFM) was used to find the thickness of the spin coated colloidal templates and untemplated cobalt samples. It was also used to estimate the height variations in the patterned cobalt samples to define their uniformity. Experiments used an Asylum research (MFP-3D) AFM and ultrasharp silicon cantilevers (μMasch CSC37/Cr-Au) with a 50 nm radius of curvature specified by the manufacturer.

The major advantage of AFM is that it gives true height measurements (as opposed to

an SEM) and also provides the advantage of imaging non-conducting solid materials without any coating. Many books are available that discuss the fundamentals of AFM.[47,48]

AFM images are obtained by using a cantilever with a sharp tip near the sample surface. The tip is fixed at a constant distance from the surface. As the tip raster scans in two dimensions (XY), a piezo-electric sensor moves in the Z direction to maintain a constant deflection using a feedback loop. Depending on the difference in the deflection value, a voltage is applied to the piezo-electric sensor to move the sample up or down to maintain the constant deflection. The voltage applied to the piezo-electric sensor plotted against the tip movement gives the true height variations on the sample surface. This provides a three dimensional image of the sample topography. The deflection of the tip is detected by a light sensitive detector sensing displacement of laser beam reflecting off the back of the cantilever. Various forces such as van der Waals, electrostatic, capillary, adhesive and double layer can act between the tip and the sample.

In the atomic force micrographs that are shown in this thesis, white regions correspond to higher regions of the sample. Image resolution in our experiments is determined by user input parameters. For example, Figure 4.20 (a) is a 512×512 pixel image of a 60×60 μm^2 scanned area, giving a maximum resolution of 8.5 pixels/μm. Typically, scan speeds were 0.2 - 0.5 Hertz.

In order to calculate thickness of the deposit using AFM, one needs to scan over an edge of the deposit, scribing the sample with a blade to get a sharp edge. Figure 4.20B shows a representative line scan over a scribed edge.

2.5 LASER DIFFRACTION

Laser diffraction was used to study the structure of our colloidal templates. It provides information regarding the lateral periodicity present in the sample, and is non-intrusive,

high-speed and high-resolution analysis.

For a transmission geometry, the diffraction equation is given by:

$$n\lambda = d\,\sin\theta, \tag{2.7}$$

where λ = wavelength of the incident light,

d = inter-planar distance,

θ = angle between the incident ray and the lattice planes (or diffraction peaks).

For Equation 2.7 to be satisfied, it is necessary that $\lambda < d$. Considering the diffraction limit ($\lambda < d$), a violet laser (λ=405 nm, 25 mW, Photonic Products, PMM-608G-VT) was used to analyze the colloidal sample with silica particles with diameters $\approx 0.5\ \mu$m. The laser beam with ≈ 5 mm diameter was spatially filtered using a pinhole and lens combination (spatial filter, Thorlabs-KT310) shown in Figure 2.2. The output beam diameter was ≈ 1.5 mm. The combination of two lenses forms an inverted telescope and the pinhole was used as a spatial filter. The diffraction pattern on a screen (a microscope slide covered with white paper) was imaged using a CCD camera (QImaging, 32-0090B-282) with a macro lens (Edmund Scientific, NT56-524). The laser diffraction from our micron-sized particles is analogous to X-ray diffraction from atoms in the solid. A diffraction pattern gives information about the symmetry present in the colloidal sample. From the peak separations for a close-packed crystal, one can also calculate the average size of the colloidal particles based on the characteristic lattice spacing.

A colloidal sample (prepared by spin coating a silica suspension in acetone at 3000 rpm) was used to study the template structure and to calculate the average diameter of the silica particles. The laser diffraction pattern consisted of four peaks, representing four-fold symmetry present in the colloidal template. Using the distance of the screen from the sample (D) and the distance between the opposite peaks (h) the angle θ was calculated using

$$\tan\theta = \frac{h/2}{D} \tag{2.8}$$

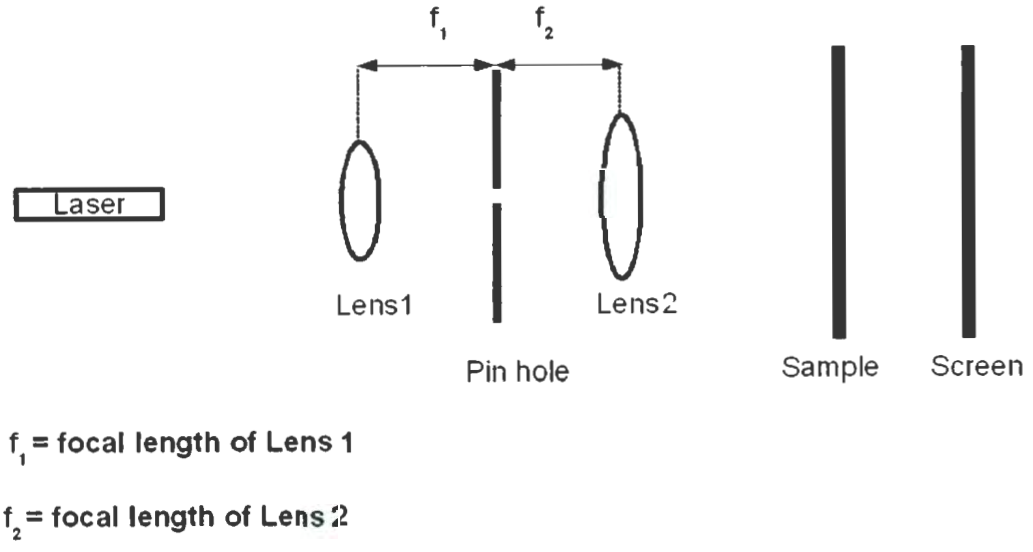

Figure 2.2: The schematic diagram of the spatial filter used for laser diffraction experiments.

Using the value of θ and Equation 2.7, the inter-planar distance (d) was calculated for the colloidal spheres arranged in (100) planes parallel to the substrate in an fcc structure for λ = 405 nm, to give an average particle diameter of 463 $\pm$ 4 nm.

Chapter 3

PREPARATION OF TEMPLATE AND TEMPLATED MATERIAL

3.1 SUMMARY

The preparation of templated cobalt samples is a multiple step procedure. At each stage it is necessary to keep the sample free from any kind of residue. Each step can be optimized only after analyzing the quality of the end-result sample produced after the electrodeposited cobalt. The general scheme for the electrodeposition of cobalt through the template is shown in Figure 3.1.

Conducting substrate preparation

Three sets of conducting substrates were prepared in order to electrodeposit cobalt through the spin coated templates: gold on glass substrates (Au/glass) and two gold on chromium on glass substrates with different gold layer thicknesses (thin-Au/Cr/glass and thick-Au/Cr/glass). In all cases, coverslips were used as the glass substrate. Without an adhesion layer of chromium, the gold peeled off the coverslips during electrodeposition. The details of substrate preparation are given in Section 3.2.

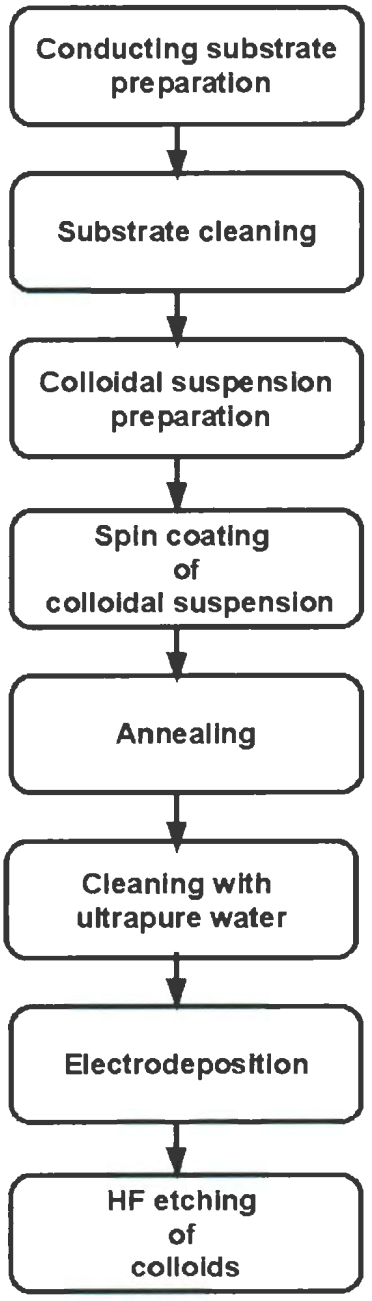

Figure 3.1: A schematic diagram showing the steps involved in the preparation of patterned cobalt by templated electrodeposition.

Substrate cleaning

Electrodeposition is very sensitive to the cleaning procedure used to clean the conducting substrates before spin coating. Using thick-Au/Cr/glass substrates, different cleaning processes were practiced to get a visually uniform deposit (see Section 3.3). The two most promising cleaning methods were acetone vapor cleaning and cleaning with H_2SO_4 (sulphuric acid).

Preparation of colloidal suspension

The next step in the synthesis of a patterned cobalt deposit is the preparation of a colloidal suspension (Section 3.4.1). The preparation of the silica colloidal suspension in acetone (20% silica spheres by total volume) is very sensitive to the preparation temperature. The colloidal suspension works best when prepared at a temperature between 24° C and 27° C.

Spin coating of colloidal suspension

The templates for electrodeposition were prepared by spin coating 37 μL of the silica suspension on the Au/Cr/glass at 3000 rpm for 30 seconds. A star-like reflection was observed on the samples within a few seconds of spin coating.

Template preparation for electrodeposition

To stabilize the templates in water for the electrodeposition step, they were annealed at an optimized temperature of 300° C for 3 hrs in a furnace with a ramp up time of 3 hrs (100° C/ hour), and removed at 300° C. Prior to electrodeposition, the templates were cleaned by dipping in ultrapure water.

Electrodeposition

One needs to optimize the parameters involved during electrodeposition to deposit a visually uniform layer of cobalt from $CoSO_4$. This optimization was done using a stainless steel strip as a working electrode (Section 3.5). One needs to add H_3BO_3, which acts as a weak buffer, to the electrolyte in order to stabilize the pH during electrodeposition. The electrodeposition through colloidal templates was carried out under the same conditions used to obtain optimal

cobalt electrodeposits on a stainless steel electrode, but the results were not good for the templates. We do not yet fully understand why.

HF etching

After electrodeposition, the prepared samples were etched with hydrofluoric acid (HF) to remove silica spheres. The samples were dipped in 1% HF until the star-like colored reflections vanished. The samples were etched for a time duration ranging from 30 seconds to 10 minutes. The etching time was not optimized because of the non-uniformity of the cobalt electrodeposits.

In this multi-step technique of preparing cobalt electrodeposits, a single parameter at one step was changed during each experiment in an attempt to get a visually uniform cobalt deposit. Even though lots of combinations and procedures were tested for each step, the reliable procedure to make a uniform cobalt deposit is still not clear. The different tested conditions at each step and the optimum conditions in certain cases are summed up in Appendix B.

3.2 SUBSTRATE PREPARATION

Electrodeposition requires a conducting substrate. The substrates used to support the templates for electrodeposition were prepared by vacuum evaporating gold over glass coverslips (22 mm x 30 mm, VWR International). Prior to gold coating, the cover slips were cleaned with concentrated H_2SO_4 and washed with ultrapure water (Barnstead Nanopure, 18.2 $M\Omega \cdot cm$) and dried in an oven. (One should take care of drying rings forming on the coverslips during the process of cleaning and washing.)

Peeling of the gold layer from the glass coverslip was observed during electrodeposition for Au/glass substartes. In subsequent experiments, a thin layer of chromium was vacuum evaporated on the glass, prior to the gold. This enhances the adhesion of gold coating on

glass. The thickness of the chromium layer was approximated to be 27 nm using a thickness monitor. (The uncertainty associated with the chromium thickness is unknown.)

To prepare thick-Au/Cr/glass, 0.1234 g of gold was loaded in to the evaporator boat located at 20 cm from the substrate holder, whereas thin-Au/Cr/glass substrates were prepared from 0.09611 g of gold evaporated from the boat fixed at the same distance. Figure 3.2 shows the difference in coating adherence on a gold coated substrate with and without the chromium underlayer. Figure 3.2 (A) shows an image of an electrodeposit (front view) and back view in Figure 3.2 (B). The region on the left has a Cr underlayer below the gold, while the region on the bottom right (to the right of the circular arc) does not. The gold peeled off the glass after Co electrodeposition without the Cr underlayer.

To make the substrates ready for electrodeposition, electrical contacts were made using Norland conductive adhesive and uninsulated wires. The coverslips were then glued with a UV glue (Norland NOA 68) to a microscope slide for structural strength and to eliminate the affect of the sucking force from the substrate-holding mechanism of the spin coater on the sample preparation. A schematic diagram of the final substrate used in our experiments is shown in Figure 3.3.

3.3 SUBSTRATE CLEANING

Electrodeposition is extremely dependent on the surface properties of the substrate, including the cleanliness of the exposed surface. It is necessary to clean the substrate at several points during the substrate preparation process. We studied the effect of different cleaning procedures on untemplated substrates used for electrodeposition, and our results are summarized in Table B.1 (Appendix B). It should be noted that we have not yet identified optimal preparation conditions for producing templated electrodeposits in a reliable manner. The electrodeposition of cobalt is sensitive to the substrate cleaning procedures prior to the spin

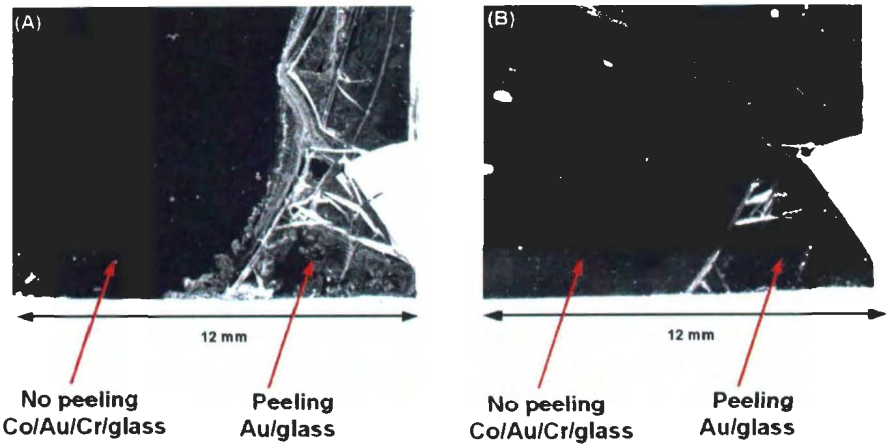

Figure 3.2: Image of an electrodeposit, front view (A) and back view (B). The gold peeled off the glass after cobalt electrodeposition in the region without the Cr underlayer, whereas almost no peeling occurred in the region with the Cr underlayer.

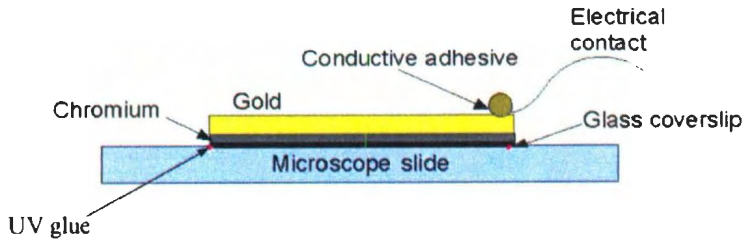

Figure 3.3: A schematic diagram of the substrate used in experiments for this thesis.

coating step. Various solvents and acids including acetone, ethanol, H_2SO_4 and acetone vapor were tried for cleaning the gold substrates. Cleaning the bare gold with pure acetone and ethanol never worked to reach the aim of uniform cobalt deposits, while H_2SO_4 or acetone vapor cleaning did give uniform untemplated cobalt deposits. However, this success did not carry through to the case of electrodeposition through a colloidal template.

3.4 COLLOIDAL TEMPLATE PREPARATION

This section explains the three major steps involved in preparation of a colloidal template: substrate preparation, colloidal suspension preparation and spin coating the colloidal suspension on the substrates.

3.4.1 COLLOIDAL SUSPENSION PREPARATION

Earlier studies have shown that the structure of a template affects the magnetic properties of a patterned cobalt array.[30] For the production of our colloidal templates, it is necessary to prepare the colloidal suspension properly.

The colloidal suspension was prepared from silica spheres (Fiber Optic Center, SIO2P050-1 microspheres of diameter 458nm $\pm$ 2 nm with less than 6% polydispersity, since no calibration standard was used, possible systematic errors in particle diameter is 5 %) in acetone (Fisher, reagent grade). The colloidal spheres were dried overnight in the oven at 150° C to remove absorbed water before using them for preparing the colloidal suspension. For the sake of reproducibility, 5 mL of 20% (by volume) colloidal suspension was prepared in a 20 mL glass bottle by ultrasonicating until opalescent reflections were seen. The temperature of the ultrasonication bath is a critical controlling parameter for the preparation of the colloidal suspension. The suspensions in acetone were prepared at temperatures ranging from 15° C to 35° C, and opalescent reflections were observed after 3-4 hours if the temperature of the

bath was maintained between 24° C and 27° C using a copper cold water circulation system. Suspensions prepared at a starting temperature higher than 27 ° C did not show any opalescent reflections after sonication for one day. Suspensions prepared at starting temperatures lower than 24° C showed opalescent reflections after sonication for two days.

The opalescent reflections from the suspension generally give a good indication that the colloidal suspension is ready to spin coat. After the appearance of opalescent reflections, the suspension was tested by spincoating it over the glass coverslips after each subsequent hour of sonication for the presence of aggregates, until a clean sample was obtained. Figure 3.4 shows samples prepared from a colloidal suspension in acetone. Figure 3.4A shows the result of spin coating the suspension sonicated for one hour after the appearance of opalescent reflections. Streaks appear on the sample due to larger aggregates moving during spin-coating. Figure 3.4B is the result of spin coating suspension sonicated for 2 hours after the appearance of opalescent reflections. The sample looks cleaner. In both cases, the suspension was left undisturbed for 20 minutes before spin coating.

3.4.2 SPIN COATING OF COLLOIDAL SUSPENSION

The final step in the synthesis of the colloidal template is spin coating the suspension over the substrates. For all the electrodeposition experiments, the template was prepared by spin coating 37 mL of 20% colloidal suspension at 3000 rpm for 30 seconds as shown in Figure 3.4. The amount of suspension required for covering the complete area of the used coverslip was calculated from the experimental procedure of Jiang *et al.*[18]

Jiang *et al* fabricated crystals by spin coating 600 μL of a suspension on a 4-inch silicon substrate. The suspension was prepared from 325 nm silica spheres in non-volatile ethoxylated trimethylolpropane triacrylate monomer (ETPTA).

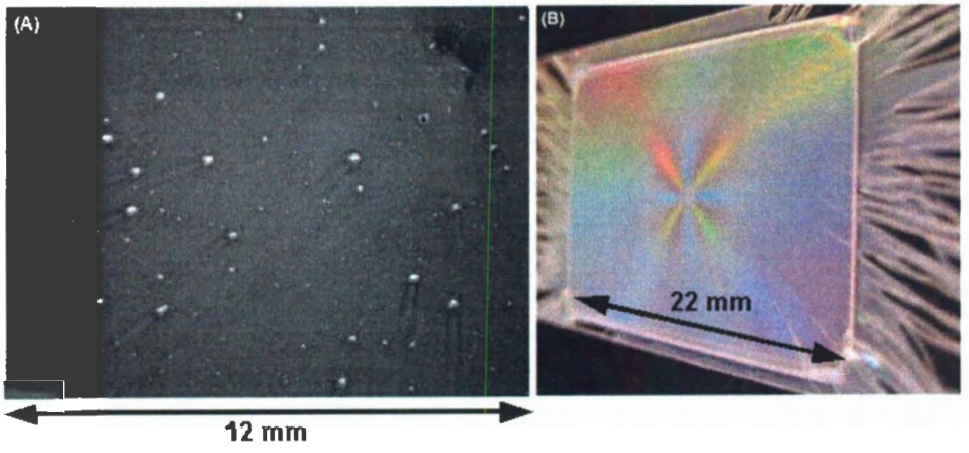

Figure 3.4: Two samples prepared from the same colloidal suspension in acetone. (A) Image of the sample taken with a CCD camera. The sample was prepared by spin coating a silica suspension sonicated for 1 hour after the appearance of opalescent reflections. The dark spot at the top right corner of the image corresponds to the spinning center of the sample. The streaks appear on the sample due to the presence of aggregates. (B) The result of spin coating a suspension sonicated for 2 hours after the appearance of opalescent reflections; this sample looks cleaner. In both cases, the suspension was left undisturbed for 20 minutes before spin coating.

3.4.3 PREPARING TEMPLATE FOR ELECTRODEPOSITION

A colloidal template coated onto a substrate is unstable in water and needs annealing treatment for stabilization prior to electrodeposition. To find the optimum annealing temperature, templates on glass substrates were annealed at different temperatures between 200° C and 600° C to find the best temperature to stabilize the templates in water. Templates annealed below 300° C dissolved in water, whereas templates annealed at temperatures above 500° C caused the glass substrate to melt. Subsequent templates were annealed using a ramp up time of 3 hours to go from room temperature to 300° C, a dwell time of 3 hours, and ramp down to 50° C in a time of 3 hours. After annealing, the templates were dipped in ultrapure water to remove any debris.

3.5 SYNTHESIS OF COBALT ANTI-DOT ARRAY BY ELECTRODEPOSITION

Cobalt was electrodeposited from 0.01 M $CoSO_4$ using a three electrode system: stainless steel as the counter electrode, Ag/AgCl (saturated KCl) as the reference electrode, and spin coated templated Au/Cr/glass as the working electrode. Cobalt was deposited with a constant applied potential (-1.2 V *vs.* Ag/AgCl) using a Hokuto Denko HA 501 potentiostat/galvanostat. The depositions were carried out in a Pyrex glass cell. After deposition, samples were rinsed with ultrapure water and then air dried.

The electrodeposition of cobalt is sensitive to the pH of the electrolyte and the distance between the counter and working electrode, along with other influencing factors like substrate cleanliness and template adherence. Rapid changes in pH were observed during electrodeposition experiments if 0.01 M H_3BO_3 was not added to the electrolyte. Boric acid acts like a buffer and stabilizes the pH of the electrolyte between 2 and 3 during the electrodeposition,

as reported by Bartlett *et al.*[31] The effect of pH was studied on the uniformity of cobalt deposit by using stainless steel working electrodes at different distances. A visually uniform deposit was obtained on the stainless steel for a distance > 2.5 cm between the electrodes. A green deposit, suspected to be cobalt hydroxide, was observed for separation distances < 2.5 cm. The cause of hydroxide formation at small distances has not been investigated.

The cobalt deposit through templates was visually non-uniform under conditions that yielded visually uniform deposits on untemplated steel electrodes. At this stage, factors like substrate cleanliness and annealing need to be optimized to improve the quality of the templated electrodeposits.

3.6 HYDROFLUORIC ACID (HF) ETCHING

Wet chemical etching with hydrofluoric acid (HF) was used to remove the silica templating colloids to get a patterned cobalt deposit with air interstitials. General procedures for etching silica colloids with HF is given in the literature.[49]

In our experiments, in order to determine the optimum time for etching colloidal spheres, 10 samples were dipped in 1% HF and 12 samples were dipped in 2% HF for different time periods ranging from 30 seconds to 10 minutes. The time required for etching depends on the thickness of the deposit. Various factors limited the reproducibility of an optically uniform cobalt deposit through colloidal templates. Thus, the optimum time for HF etching was not estimated. However, these preliminary results suggest that, samples etched for 2 - 3 minutes in 1% HF show some good templated regions by SEM.

Chapter 4

DATA ACQUISITION AND ANALYSIS

4.1 SYMMETRIES

A colloidal crystal composed of 0.5 μm spheres exhibits colorful white-light Bragg reflections. When white light is incident on a colloidal crystal at a certain angle, it satisfies the Bragg reflection condition for a specific wavelength. Thus, reflections from a single crystal at a given incidence angle are observed to have a uniform color. Dip coating is a standard technique to produce colloidal crystals. However, the regions where one gets good crystals is hard to control. Colloidal crystals prepared by dip coating consists of mm-scale single crystal domains arranged in different orientations and are separated by grain boundaries. Reflections from single domains are observed as a solid color, and at a given viewing angle, different domains have different reflection colors, which change abruptly at the grain boundary. Spin coated colloidal crystals are different. When spin coated samples are held at an oblique angle with respect to the white light source, the reflections take the form of 4-fold and 6-fold symmetric arms that emanate radially from the center of symmetry (spinning center)

for samples prepared by evaporation from acetone and ethanol solvents respectively (Figure 4.1). These reflection patterns extend uniformly throughout the entire (cm-scale) sample. The symmetry of the star pattern (the number of arms of a star) depends on the spin speed and the solvent involved in the preparation of a colloidal suspension. The symmetry of the star-pattern is also affected by the sucking force from the substrate-holding mechanism of the spin coater. This affect is eliminated by gluing the coverslip on a microscope slide, which provides mechanical strength and avoid bending of substrate due to sucking mechanism.

4.1.1 SOLVENT DEPENDENCE

For a particular speed and concentration of the prepared suspension, the symmetry of the star pattern varies with the type of solvent used for making the colloidal suspension. The four-arm star pattern in Figure 4.1A resulted from spin coating a colloidal suspension in acetone at 3000 rpm. A six-armed star pattern was observed for the samples prepared from a colloidal suspension in ethanol, spin coated at the same spinning speed (Figure 4.1B).

4.1.2 SPIN SPEED DEPENDENCE

There were symmetry transitions as a function of spin speed (Figure 4.2). The speed was varied in increments of 500 rpm. In the case of a colloidal suspension prepared in acetone, a four-armed white light reflection pattern was observed at spin speeds from 3000 rpm to 5500 rpm (Figure 4.3A: Four-fold-1). When the colloidal suspension was spin coated at 6000 rpm, a six-armed star was observed (Figure 4.3A: Six-fold). At spin speeds between 6500 rpm and 7500 rpm, a broad (re-entrant) transition from six-fold to four-fold symmetry was observed (Figure 4.3A: Mixed). Samples showed a four-arm star near the spinning center, diverging into six arms extending toward the edges of the substrate (Figure 4.3A). Figure 4.3B shows red and green channels of a color RGB image of a sample with mixed symmetries: the green

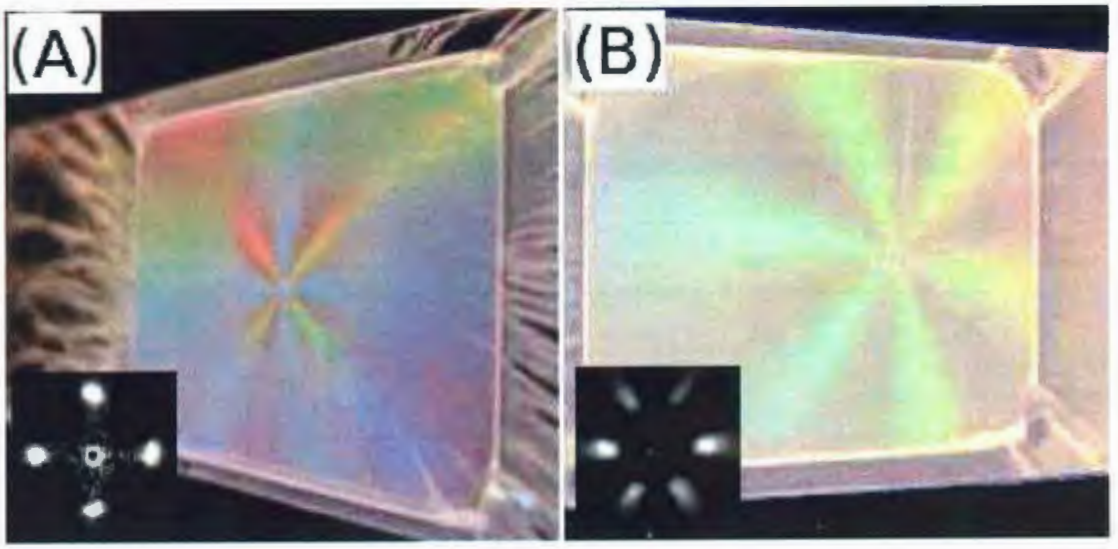

Figure 4.1: White light reflections on a sample prepared by spin coating a colloidal silica suspension (20% silica in total volume) at 3000 rpm prepared in (A) acetone and (B) ethanol solvents (onto 22 × 30 mm coverslips) display 4-fold and 6-fold symmetric patterns that extend across the entire sample. A laser beam passing through the sample results in diffraction patterns (insets) which demonstrate that 4-fold or 6-fold symmetries are present in the samples.

channel highlights six-fold symmetry near the edges of the sample, while the red channel shows 4-fold symmetry near the center.

The spin coating of a colloidal suspension in ethanol resulted in a six-arm star pattern for all spin speeds between 3000 rpm to 7500 rpm, and four arms at the spin speed of 8000 rpm (Figure 4.2B: Ethanol).

4.2 STRUCTURE OF FOUR-FOLD SYMMETRIC COLLOIDAL TEMPLATES

A high degree of order in spin coated colloidal films was initially expected due to the presence of a single four-arm or six-arm reflection pattern over the entire sample. Scanning electron microscopy (SEM) (described in Section 2.3) was used to analyze the order and to understand the origin of the symmetry present in the real space structure of a spin coated colloidal film. The colloidal sample used for structure analysis was prepared by spin coating from a silica suspension in acetone (20% silica in total volume) at 3000 rpm. Much of the work in this section has been published by us.[21]

4.2.1 SEM ANALYSIS

The SEM analysis showed that in the case of samples prepared by spin coating from a colloidal suspension in acetone, the silica colloidal spheres are packed in a [100]-oriented fcc structure (Figure 4.4B) , consistent with the four-armed star feature (Figure 4.4A). Small domains with [111] packing (marked by arrows in Figure 4.4B) appeared to connect the [100]-packed regions.

The real space picture from SEM revealed the polycrystalline nature of the sample, contrary to previous suggestions by Jiang *et al.*, that the spin coated colloidal crystals are

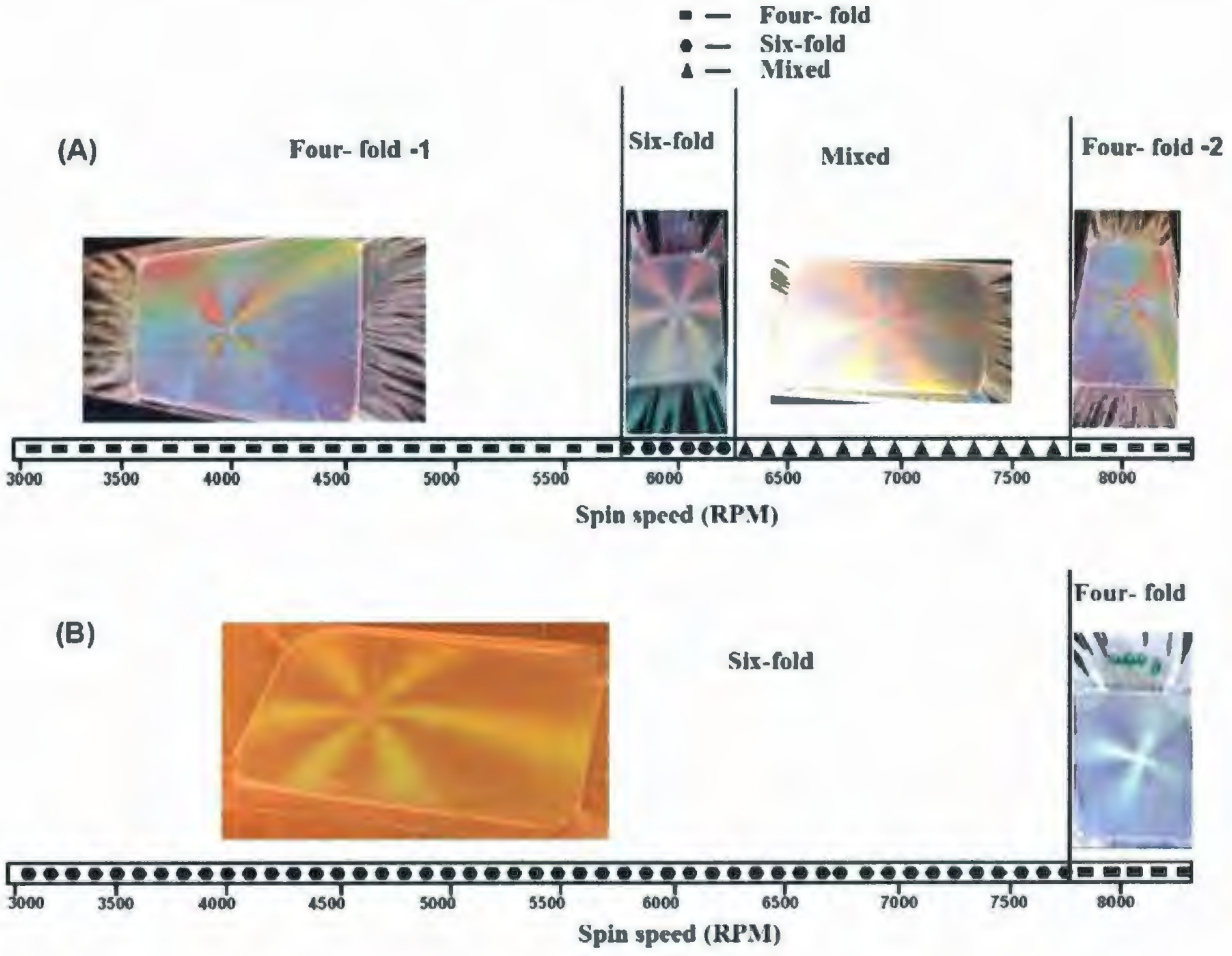

Figure 4.2: The number of arms observed in a spin coated sample depends on the spin speed and the solvent involved in the preparation of the colloidal suspension. (A) Symmetries as a function of spin speed for evaporative spin coating from the silica colloid suspension in acetone. (B) Symmetries as a function of spin speed for evaporative spin coating from a silica colloid suspension in ethanol. More than 15 samples were studied at each spin speed for a particular solvent. The samples at different spin speeds for both solvents were prepared on a same day as well as on different days to check the reproducibility of the results.

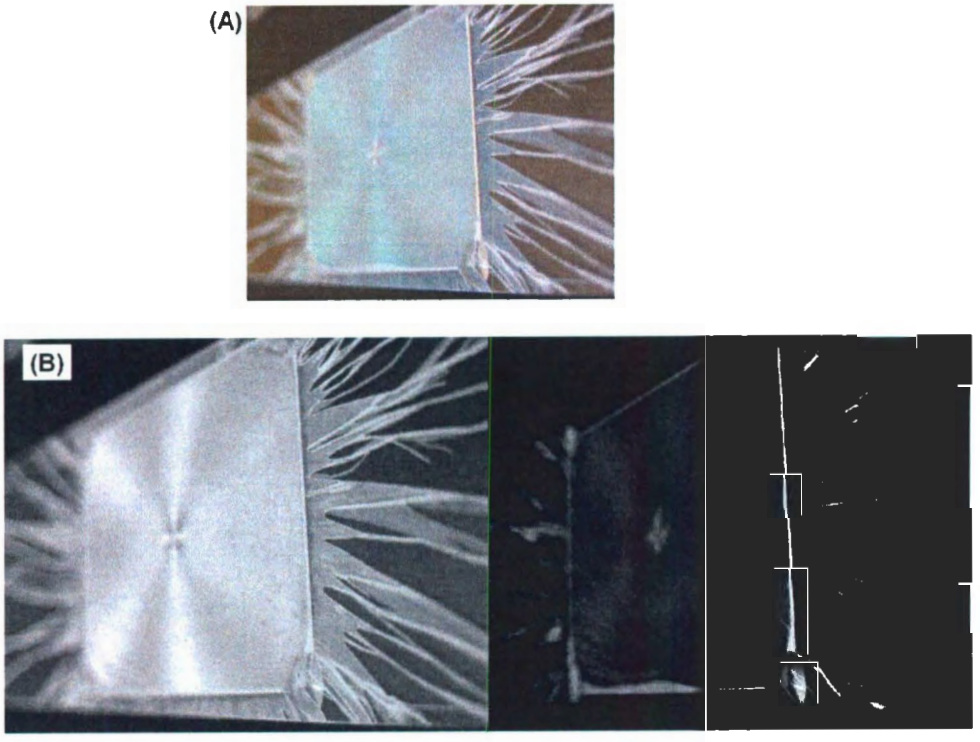

Figure 4.3: (A) A sample prepared at 7000 rpm by spin coating a colloidal suspension in acetone (onto 22 × 30 mm coverslips). The sample shows a four-arm cross near the spinning center and six arms away from the spinning center. (B) Green (left) and red (right) channels of a color RGB image of a sample with mixed symmetries: the green channel highlights six-fold symmetry near the edges of the sample, while the red channel shows four-fold symmetry near the center.

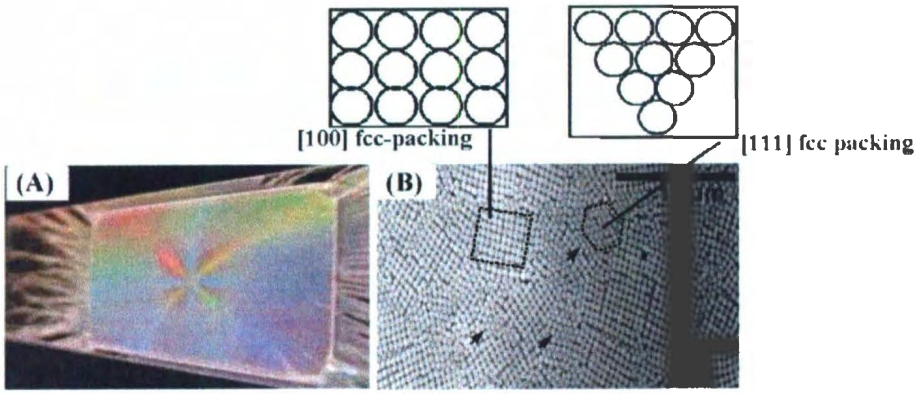

Figure 4.4: (A) A photograph shows a sample prepared by spin coating a silica suspension (20% silica in total volume) in acetone at 3000 rpm (onto 22 × 30 mm coverslips). (B) An SEM image of this shows that the silica spheres are packed in a [100]-oriented fcc structure. Regions with [111]-packing (marked by arrows), connect the [100]-oriented regions.

single crystalline.[18] The results by Jiang *et al.* (on six-fold symmetric samples) were based on SEM analyses of regions far away from the spinning center, where the presence of larger domains is expected. Their results were interpreted from Fast Fourier Transforms (FFTs) of SEM images taken at four equidistant spots from the center of spinning, but in different directions (see Figure 3 in Jiang *et al.*[18]).

We performed careful analyses of SEM images, taken as a function of distance from the spinning center. For the sake of positional accuracy, a piece of the sample was cut in a triangular fashion, with one vertex as the spinning center. SEM images of regions separated by 0.5 mm were taken, beginning at the center of spinning (one vertex of the triangle), and ending at the edge of the sample. The FFT of SEM micrographs at the center of spinning showed a diffuse ring, suggesting the absence of crystalline order. Peaks in the FFT of SEM images first emerge for scans obtained at a radial distance of 1.5 mm from the center. The orientation of the peaks was unchanged while moving radially outward in the sample, in spite of having crossed $\approx$ 1000 single-domain grains; thus we conclude that an orientational registry is maintained in the radial direction. An image stack with FFTs of SEM images obtained along the line from the center of spinning to the edge of the sample is shown in Figure 4.5. It is noticeable that the SEM images and their FFTs are stretched. The stretching might be because of poorly attached sample on the stage (or plate) and/or charging of the sample during imaging. The peaks in the FFTs are not sharp spots, but have an angular spread. The angular spread is related to the orientation of the domains in the imaged region. The angular spread decreases with the radial distance (e.g. $10^\circ \pm 2^\circ$ and $8^\circ \pm 1^\circ$ for the samples at radial distance 3.5 mm and 9.5 mm), which suggests that the domain size increases far away from the spinning center (Figure 4.6).

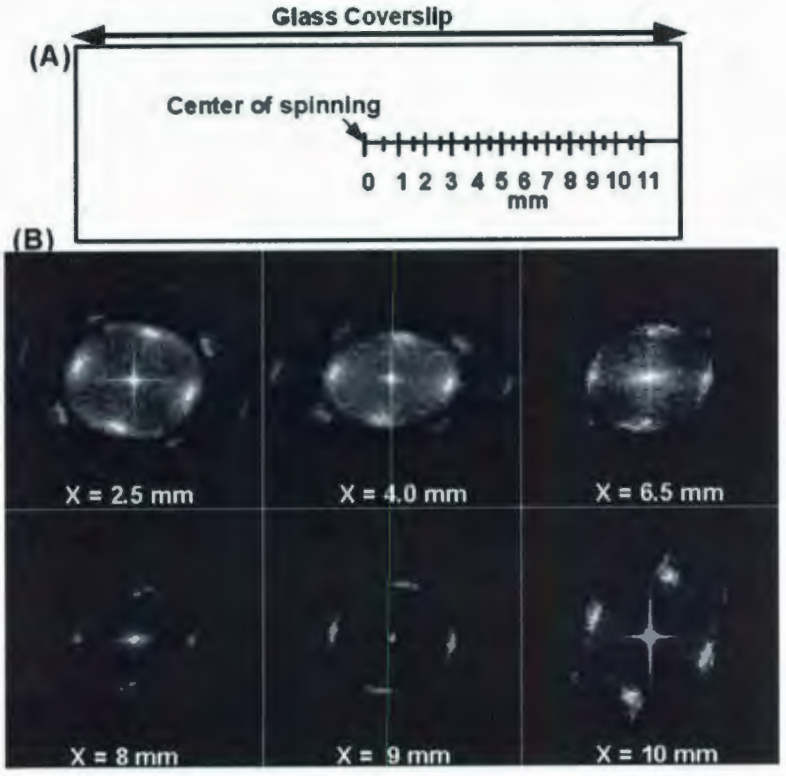

Figure 4.5: (A) Scanning electron micrographs were taken at equidistant points along a line from center of spinning to the edge of the sample. (B) shows a Fast Fourier Transform of an SEM image for a sample prepared by spin coating silica suspension in acetone at 3000 rpm, taken outward from the center of spinning along a radial line. The relative peak orientations remain unchanged.

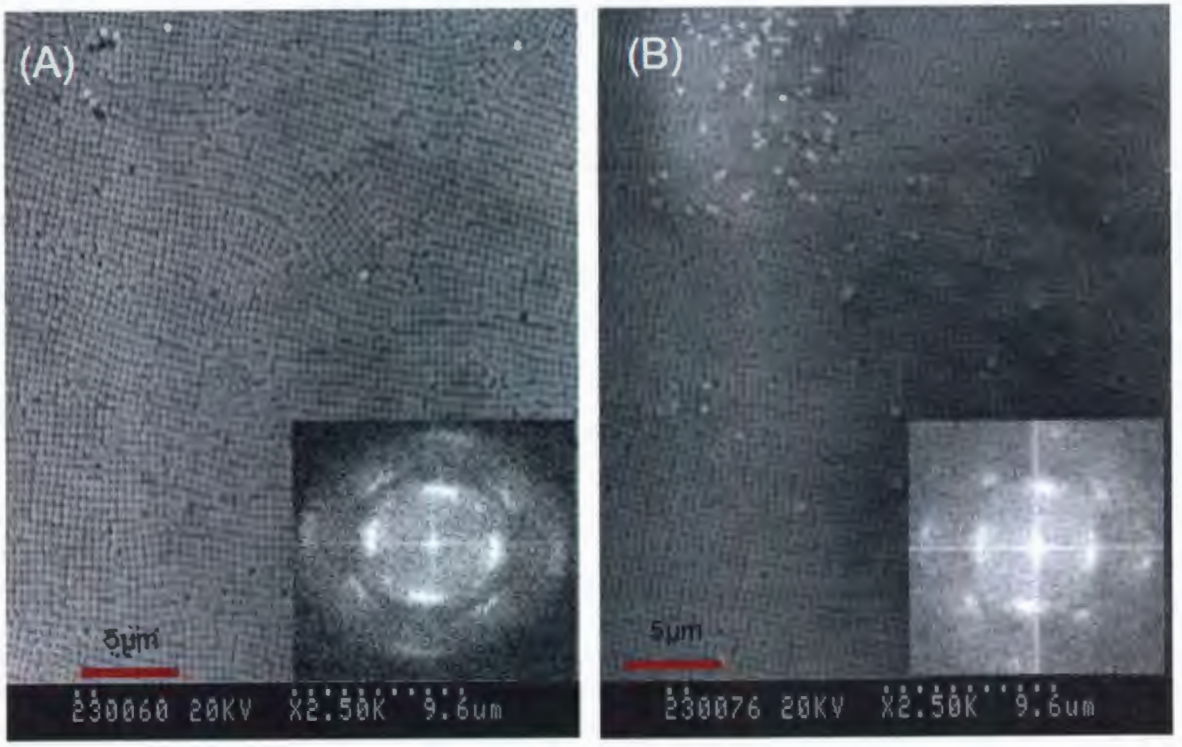

Figure 4.6: SEM images obtained at predetermined positions along a radial direction, (A) 3.5 mm and (B) 9.5 mm from the center of spinning. Both images show strong orientational registry in their FFTs (insets). The angular spread in the peaks decreases from $10° \pm 2°$ to $8° \pm 1°$ while moving outward in the sample, suggesting the presence of larger domains near the edge.

4.2.2 LASER DIFFRACTION

The laser diffraction was primarily used to find the lattice spacing in the colloidal templates and diameter of the used silica spheres (Section 2.5). We used results from both scanning electron microscopy and laser diffraction to study the structure of spin coated colloidal films. Unlike scanning electron microscopy, laser diffraction probes larger areas using a millimeter-diameter laser spot. The optical set up is explained in Section 2.5. Laser diffraction patterns obtained from samples, prepared by spin coating from a colloidal suspension prepared in acetone or ethanol at 3000 rpm shows four-fold symmetry (Figure 4.7A) and six-fold symmetry (Figure 4.7B) respectively. Consistent with the observations from SEM, the region at the

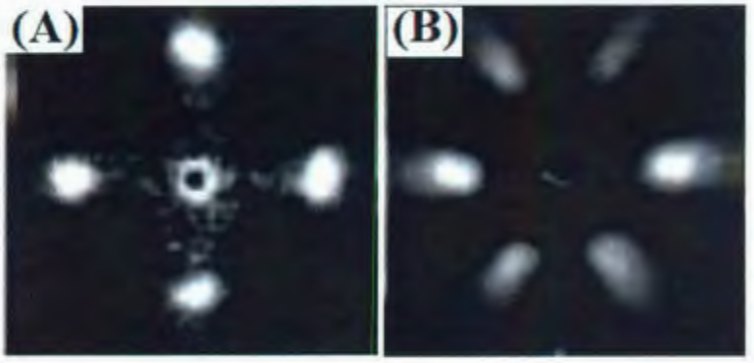

Figure 4.7: Laser diffraction patterns obtained from samples, prepared by spin coating from a colloidal suspension prepared in acetone or ethanol at 3000 rpm shows four-fold symmetry (A) and six-fold symmetry (B) respectively. The primary transmitted laser spot was blocked by a piece of black paper.

center shows no diffraction peaks. The diffraction pattern at the center of the sample has circular symmetry and has an average domain size much smaller than the laser spot size. A first-order diffraction pattern with bright peaks appears for all distances $\geq$ 2.5 mm. This shows that, although the area illuminated by the laser spot contains a large number of domains oriented in different directions, there exists an average crystalline orientation giving

rise to the diffraction pattern. From this, one can deduce the upper limit on the size of domains.

4.2.3 LATERAL AND ANGULAR SPREAD: UPPER LIMITS ON DOMAIN SIZE

We assume that the diffraction maxima are observed clearly only when some sizeable fraction of the diameter of the sample spot (f) illuminated by the laser consists of a region (made up of large number of domains oriented in different directions) with an average direction of periodicity. In stating the above assumption we establish the following:

- To observe the laser diffraction pattern at a radial distance r from the center of spinning using a laser beam with a 1.2 mm diameter, the sample spot illuminated by the laser should contain a region (consisting of correlated domains of finite size) extending laterally by a distance, $d \approx 1.2 \times (f) = 1.2 \times f$ mm.

- The maximum angular spread ($\Delta\Theta$) in such a region at a radial distance r is d/r.

- In our sample, diffraction peaks were observed at the radial distance ≥ 2.5 mm from the center of spinning (Appendix C, Figure C.1). At all distances $r \geq 2.5$ mm (where diffraction spots are observed), the maximal angular spread of $\Delta\Theta$ implies that the tangential extent of the angular-correlated region cannot exceed $r\Delta\Theta$. We quantitatively measure the domain angular spread $\Delta\Theta$ later in this section and calculated $f = 0.5$. Thus, using the same calculations and $f = 0.5$, for a distance of 11 mm away from the center, the lateral extent of the region with average direction of periodicity could not exceed ≈ 3 mm.

The lateral extent of the region with the average direction of periodicity puts an upper limit on the laser beam diameter that can be used to observe the diffraction peaks. For

larger beam diameter one will need to go farther out radially to see the peaks. From the typical single-domain size (10 μm) seen in our SEM images, the footprint of the laser spot would contain 10^3- 10^4 single domains. The above discussion explains the interpretation of the single crystalline nature of spin coated colloidal crystals fabricated by Jiang *et al.*[18] Their SEM images were taken at 4 cm away from the spinning center, where one expects the presence of bigger regions (with average periodicity) with a lateral extent of $\approx$ 1 cm. The large single domains in SEM images at 4 cm by Jiang *et al.*[18] provided the incorrect inference that the entire sample was single-crystalline. One would expect that the orientation of the diffraction peaks would stay unchanged throughout the sample if it is a single crystal, whereas an abrupt change in peak orientation is expected if the sample is polycrystalline.

To further study the crystalline nature of the sample and the orientational correlations, laser diffraction patterns were studied by moving the laser along the radial direction from the center of spinning and away from the center (off-center) in a straight line. The diffraction pattern rotates with the circular translation of laser spot over the sample (Figure 4.8). The positions of the peaks (orientation) were fixed when the laser spot was moved along a radial direction (Appendix C, Figure C.1B). When the laser spot was moved off-center in a straight line, the diffraction pattern rotated continuously (Appendix C, Figure C.2B).

One can quantify the orientational correlation in a crystal by studying the angular correlations between the diffraction patterns obtained at different positions on the template. The laser diffraction patterns were imaged upon continuous translation of the laser by 1 mm in the x direction, radially and off-center across the sample. Considering the spinning center at (x, y)= (0,0), diffraction patterns were saved for y = 0 mm (Appendix C, Figure C.1B), y = 4 mm (Appendix C, Figure C.2B), y = 5 mm (Appendix C, Figure C.3B) and y = 7 mm (Appendix C, Figure C.4B) at consecutive x coordinates upon corresponding translation.

In order to calculate the angular correlation and cross correlations, image analysis code was used. (The correlation analysis was carried out by Prof. W. González-Viñas at the

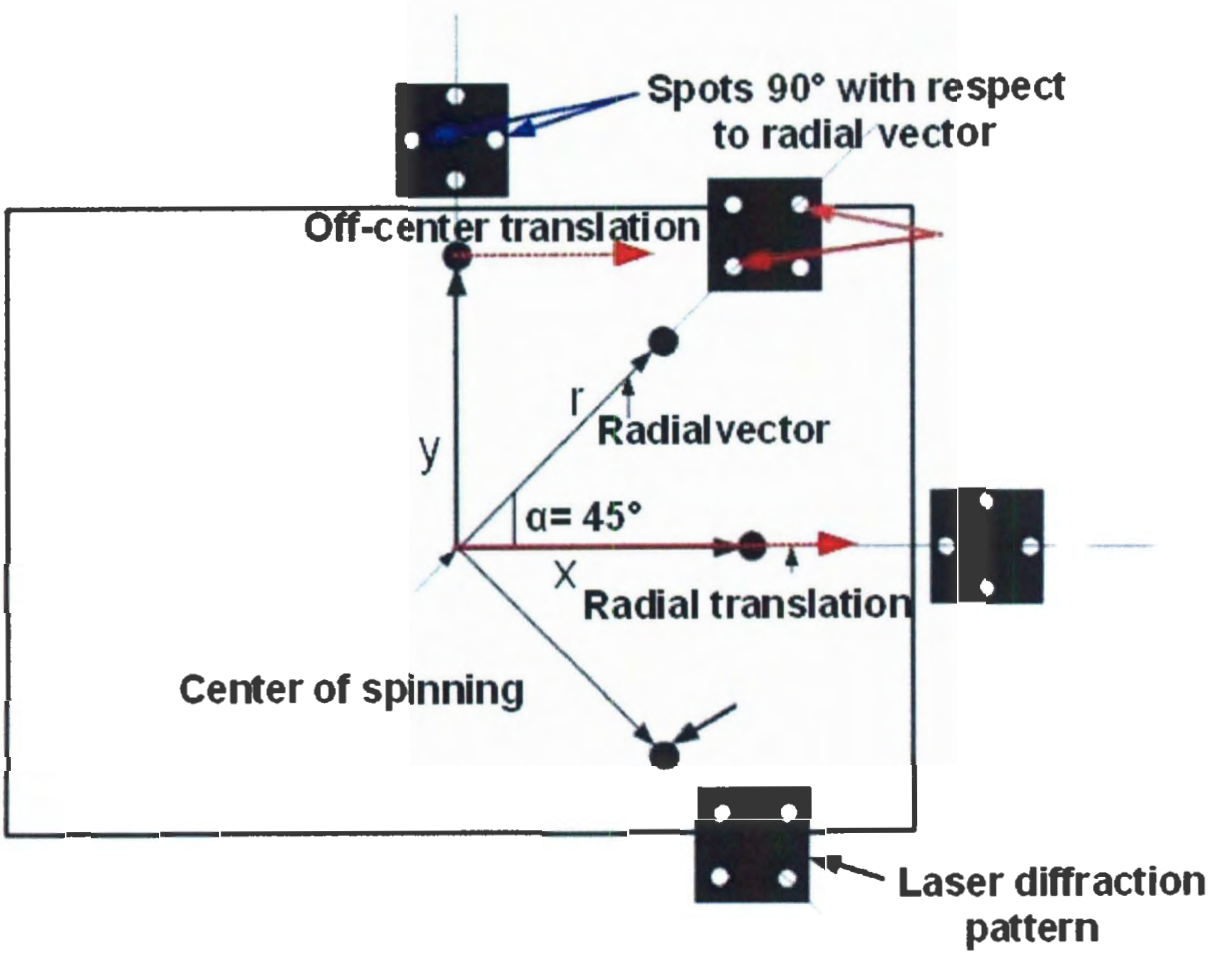

Figure 4.8: The orientation of diffraction peaks changes with the location of laser spot on the sample. The diffraction pattern rotates with the circular translation of laser spot over the sample. The coordinates (r,α) locates the laser spot on a sample.

University of Navarra.[21]) The image analysis code requires the center of the diffraction pattern to be the center of the image. All diffraction images were modified accordingly, using another image processing software (Interactive Data Language, IDL). A code was written in IDL to find the center of the diffraction pattern, and coordinates of the center were used to crop images to a particular size (465 × 465 pixels), such that the image center coincides with the center of the diffraction pattern. In order to calculate the angular correlation function, the variables (r, α) were used to locate the position of the laser spot on the sample. The reciprocal space coordinates (ρ, φ) are used to define the position of the laser spots (diffraction maxima) on the screen with center as main beam.

4.2.4 PROCEDURE FOR OBTAINING AN ORIENTATIONALLY DEPENDENT INTENSITY TO CHARACTERIZE SYMMETRY

The devised procedure for obtaining an orientationally dependent intensity to characterize symmetry present in the sample (and described first in Arcos *et al.*[21]) was as follows:

- Since there are only first order maxima at some distance (say $\rho = \rho_0$), the radial average intensity is computed by integrating from ρ_0 - Δ to ρ_0 + Δ (where Δ should be sufficiently bigger than the peak extent).
- The resulting radially-averaged intensity is only a function of φ. Call it g(φ).
- However, each image is obtained at a real-space location (r, α) and we have several images at different (r, α). Therefore, we can calculate the function g(φ) for each (r, α) location. Call this function $f_{r,\alpha}(\varphi)$.

For a crystal having square symmetry ([100]-oriented fcc packing) the maxima in function $f_{r,\alpha}(\varphi)$ are separated by $\Delta\varphi \approx 90°$.

4.2.5 PROCEDURE FOR CALCULATING CROSS-CORRELATIONS

- The cross correlation of two diffraction patterns was calculated by rotating the diffraction pattern ($f_{r,\alpha}(\varphi)$) by an angle θ, ($f_{r,\alpha}(\varphi+\theta)$) to maximize a function $G(\theta; r, \alpha, r', \alpha')$, $G(\theta; r, \alpha, r', \alpha') = \langle f_{r,\alpha}(\varphi)\ f_{r,\alpha}(\varphi + \theta)\rangle$.

- The angle θ_{max} that maximizes $G(\theta; r, \alpha, r', \alpha')$ gives the relative orientation between the two diffraction patterns.

- One way of visualizing the cross-correlation is by rotating the diffraction patterns to align the peaks by eye (Figure 4.9). The above procedure to obtain θ_{max} is simply a numerical scheme to obtain this rotation angle.

- The rotation angle $\alpha' - \alpha$ was calculated for diffraction patterns obtained at all real space locations (x, y) with $(0, y)$ as the reference (except for $y = 0$, where the reference was at the edge).

The graph shown in Figure 4.10 shows the agreement between $\alpha' - \alpha$ and θ_{max}. For radial translation, $\theta_{max} = \alpha' - \alpha$ was consistently zero. The rotation angle was adequately fit by $\theta_{max} = \alpha' - \alpha$ for diffraction patterns obtained upon off-center translation. For the diffraction patterns obtained from laser spot positions (4,4), (5,5) and (7,7) on the sample, rotation by 45° was required to bring them in registry with the diffraction patterns at (x, y)= (0,4), (0,5) and (0,7) respectively. The function $G(\theta; r, \alpha, r', \alpha')$ was maximized for these diffraction patterns for $\theta_{max} = 45°$. This suggests that (x, y) coordinates and θ_{max} satisfy the equation $\tan(\theta_{max}) = y/x$. In fact, for all (x, y), θ_{max} satisfies the tangent equation, confirming circular symmetry in the sample. In summary, the rotation of the diffraction pattern by an angle θ_{max} returns the diffraction pattern to the $x = 0$ orientation.

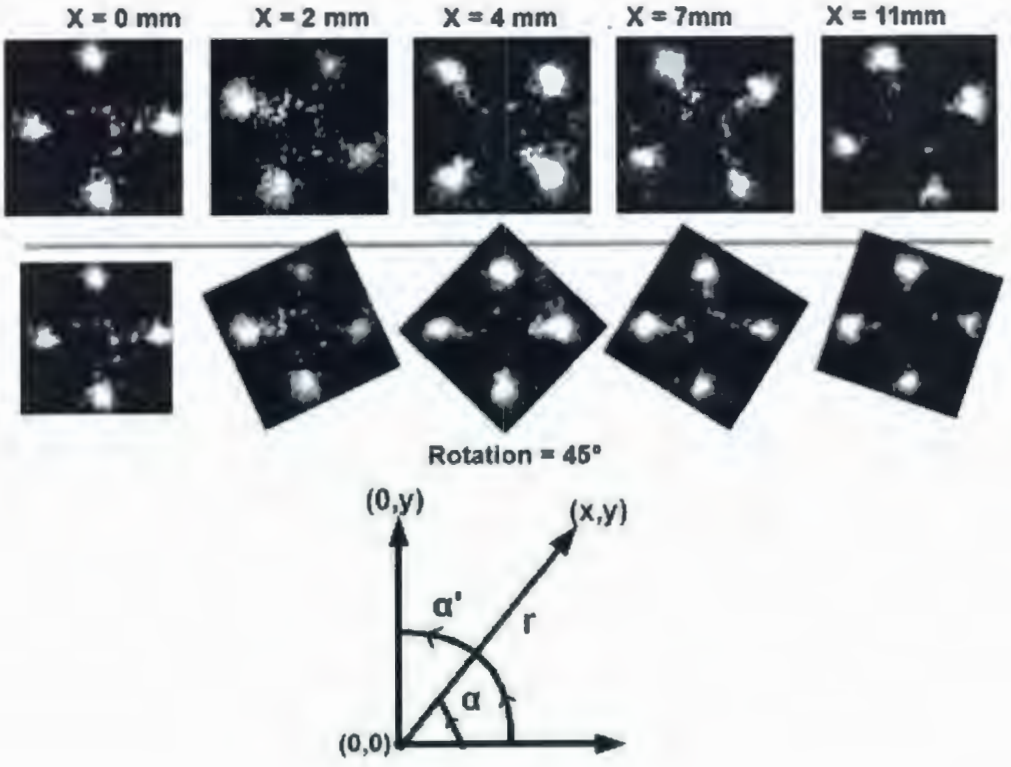

Figure 4.9: Rotation of the diffraction pattern by an angle θ_{max} returns the diffraction pattern to the $x = 0$ orientation. This continuously increasing rotation angle demonstrates the progressive rotation of the domain orientation with off-center translation. (Arcos *et al.*[21])

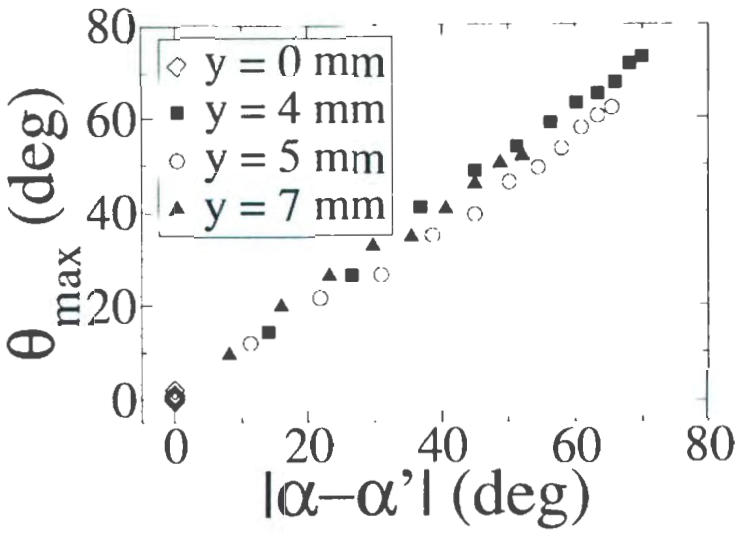

Figure 4.10: A plot of θ_{max} against $|\alpha - \alpha'|$ (sample orientation relative to the $x = 0$ orientation) shows a linear increase with unit slope, consistent with the proposed orientationally correlated polycrystalline (OCP) structure (Arcos *et al.*[21]).

Our colloidal crystals, with $\approx$ 10 μm scale domains are definitely polycrystals. However, these polycrystals show long range orientational correlations. Hence, we call it an Orientationally Correlated Polycrystal (OCP). This continuously increasing rotation angle demonstrates the progressive rotation of the OCP region with off-center translation. Along the radial direction the orientation of the OCP region stays the same. A structure consistent with these observations is shown in Figure 4.11.

4.2.6 CALCULATION OF DOMAIN ORIENTATIONAL DISPERSION

The autocorrelation function was calculated to measure domain orientational dispersion in the laser diffraction peaks.

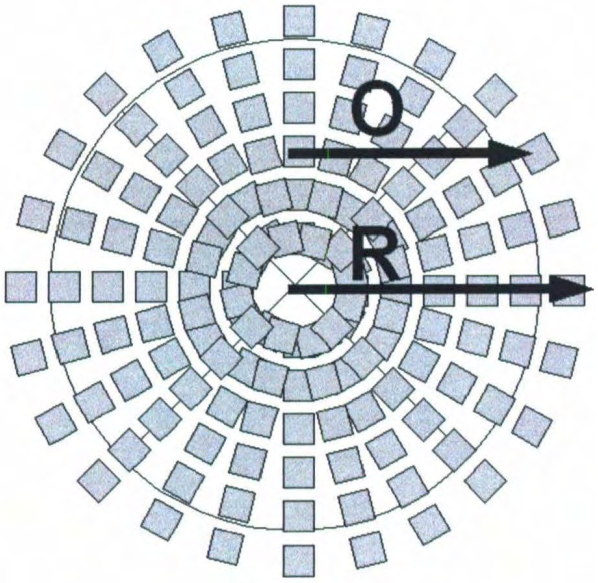

Figure 4.11: A sketch shows the proposed structure of the orientationally-correlated polycrystal (OCP): grey squares represent small OCP regions in the radial orientational registry (Arcos *et al.*[21]). "O" represents off-center and "R" represents the radial direction in the sample relative to the center of spinning.

- The correlation of a laser diffraction image with itself upon rotation is calculated by the autocorrelation function of the peaks function, $G(\theta; r, \alpha) = \langle f_{r,\alpha}(\varphi) f_{r,\alpha}(\varphi + \theta) \rangle_{\varphi}$.

- The diffraction pattern was rotated by an angle θ to maximize the value of $G(\theta; r, \alpha)$.

- The half width at half height of the $\theta = 90^{\circ}$ correlation peak gives the value of domain orientational dispersion ($\Delta\theta$).

- The domain orientational dispersion ($\Delta\theta$) was calculated for all diffraction patterns (Figure 4.12).

The value of $\Delta\theta$ decreased from 27 ° at the center to $\approx 13^{\circ}$ for the distances greater than 2mm. Note that the value $\Delta\theta = 13 \pm 1$ ° is consistent with the angular spread $\Delta\theta = 0.25$ radian ≈ 14 ° inferred earlier from the radial distance at which peaks first emerge (Section 4.2.3). Small regions are orientationally correlated with each other, such that they give rise to four-fold or six-fold reflections.

The origin of the four-fold cross in [100] oriented samples is as follows. For large source and observer distances, any point along a radial line and the radial line perpendicular to it satisfy almost the same optical condition - orientation of a crystallite is the same and the angle of the reflected beam to the observer's eye and the angle of incidence are almost the same. For a four-fold symmetric pattern, there are positions on a locus of points corresponding to a 4-arm cross that have the same position.

These observations are consistent with the SEM results, where the clear peaks in FFT analyses were visible for distances ≥ 2.5 mm from the center of spinning. The SEM studies and laser diffraction measurements showed that a spin coated template with a visible 4-arm star consists of regions with small domains. These regions are arranged in a circular fashion, as shown in Figure 4.11. For [100]-oriented fcc packing, square OCP regions satisfy the same Bragg condition (*i.e* reflections at a given angle have a preferred wavelength) in four

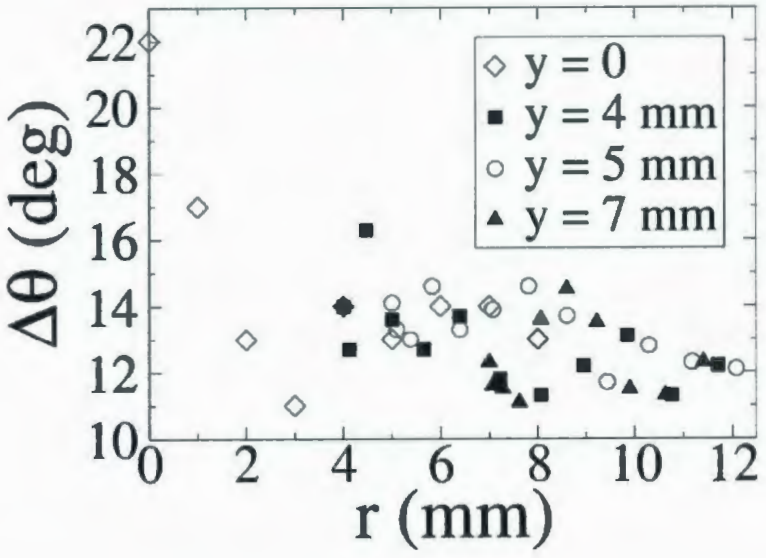

Figure 4.12: The domain orientation dispersion $\Delta\theta$ saturates at 12 ° - 14 ° as a function of radial distance (Arcos *et al.*[21]).

directions perpendicular to each other, as the angle of reflected beam to the observer's eye and the angle of incidence is always same for the observer at large distance and inter-planar distance (d) is same for four perpendicular directions. Figure 4.13 shows cross-hatched symbols that represent lattice planes in two mutually perpendicular directions with equal interplanar spacing.

4.3 SIX-FOLD SYMMETRIC COLLOIDAL TEMPLATES

A sample prepared by spin coating silica suspension in ethanol at 3000 rpm was used to study the six-fold symmetric colloidal templates. Figure 4.14 shows the type of packing present in one such sample. The packing was [111]-oriented fcc (Figure 4.14B) in the ethanol samples with a six-armed star (Figure 4.14A). Figure 4.14C shows an SEM image in another region of the sample. Small domains with [100] packing appeared to present in large numbers

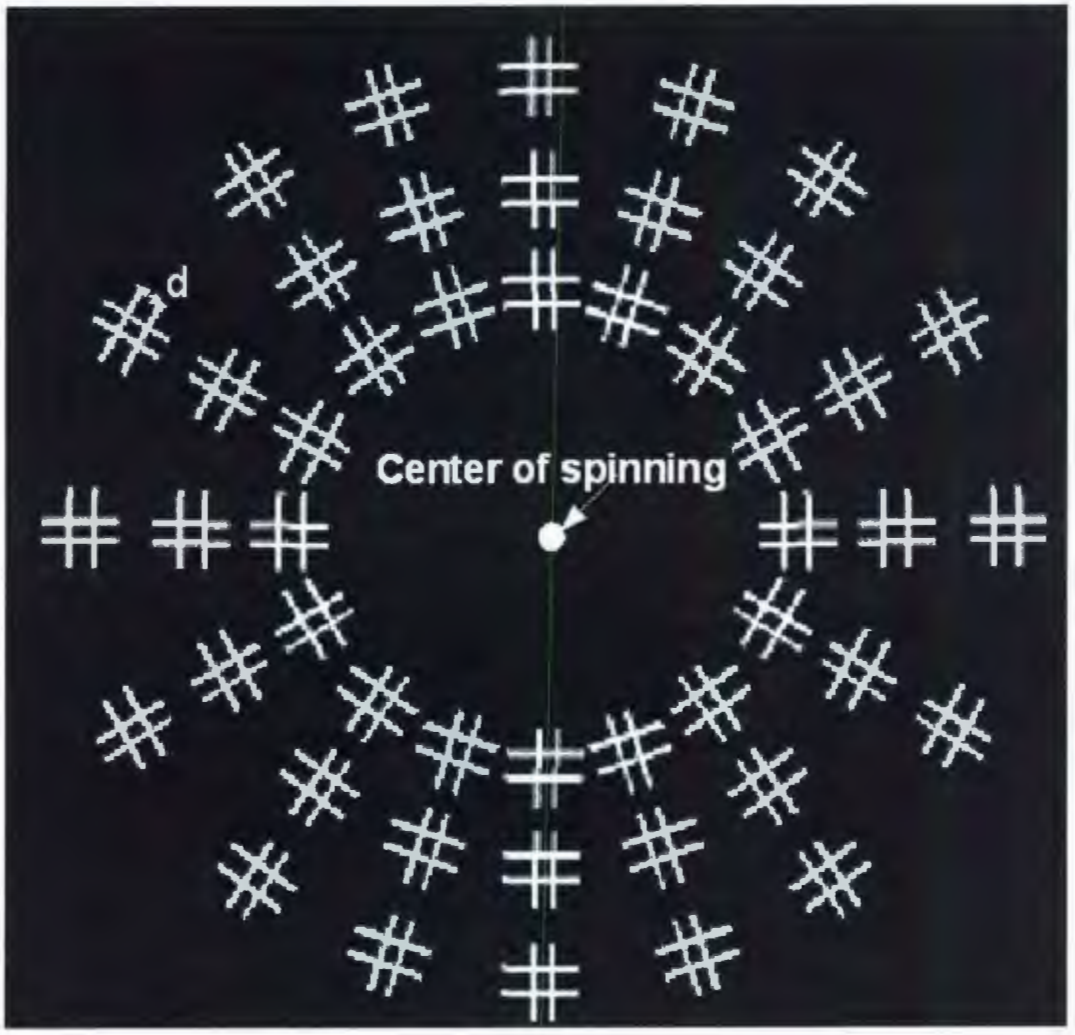

Figure 4.13: The Bragg condition will be satisfied in four directions perpendicular to each other as the angle of reflected beam to the observer's eye and the angle of incidence is always same for the observer at large distance and the inter-planar distance (d) is same for four perpendicular directions. The cross-hatched symbols represent lattice planes in two mutually perpendicular directions with equal inter-planar spacing (d).

(marked by arrows), more so than the number of [111]-oriented domains in [100]-oriented fcc structures (See Figure 4.14B). A laser diffraction of the sample is shown in Figure 4.7B. As

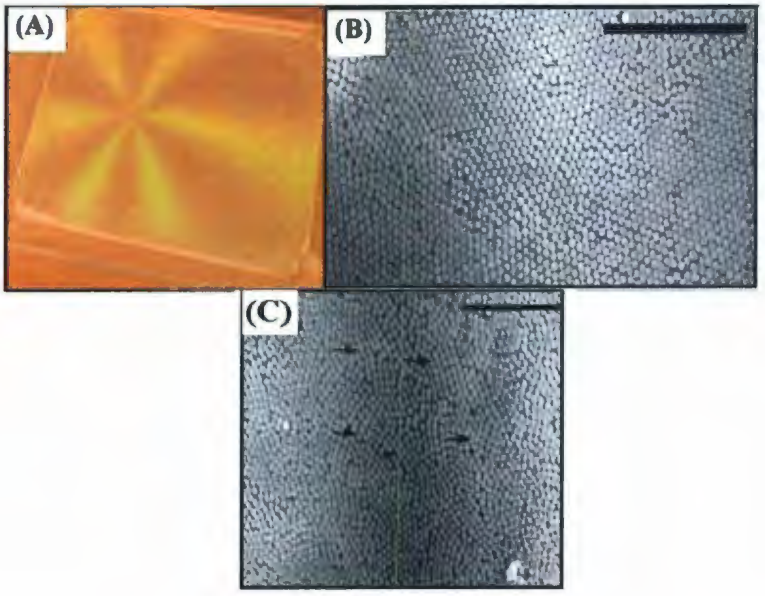

Figure 4.14: (A) A photograph shows the six-fold symmetry present in samples prepared by spin coating silica suspension in ethanol at 3000 rpm. (B) The six-fold symmetric arms (shown in A) correspond to silica spheres packed in a [111]-oriented fcc structure, according to SEM images. (C) Other regions in the same sample show small domains with [100] packing present in large numbers (marked by arrows).

explained for four-fold symmetric samples (Section 4.2), the optical cross pattern arises from the fact that the same optical condition is satisfied - there are six equivalent orientations of [111]-packed crystallite with respect to the angles of incidence and reflection. The locus of such points corresponds to a 6-arm cross.

However, laser diffraction carried out on samples prepared from colloids in ethanol suspension did not show clear Bragg spots except in rare regions in the sample where the pattern consist of six spots with two opposite spots being perpendicular to the radial direction (Figure 4.7). We interpret this as follows: the six-fold symmetric samples consist of

small [111]-packed regions connected by large [100]-packed regions, so it is difficult to find large [111]-packed regions in the samples having a clean laser diffraction pattern with our 1.2 mm beam diameter. We conclude that the orientationally correlated regions were much smaller than the laser beam diameter.

4.4 MIXED SYMMETRY COLLOIDAL TEMPLATES

While the reason for the symmetry transitions (between 4-fold and six-fold) is so far not known, it appears that at the transition, one can create samples with multiple symmetries as a function of the radial distance from the spinning center. In the case of mixed symmetry samples, the packing was [100] near to the center of spinning (which corresponds to the four-arm star pattern on the sample and four peaks in the FFT; Figure 4.15B). The [100] packing was surrounded by big regions with [111]-packing in the sample. The six-arm star pattern on the sample and six peaks in the FFT are shown in Figure 4.15C. This corresponds well with the observation of a four-arm star near the center, but a six-arm star away from the spinning center in mixed samples (Figure 4.3). Laser diffraction studies were not done on the mixed symmetric samples because of the laser beam diameter was larger than the width of the four-fold region.

4.5 THICKNESS OF COLLOIDAL TEMPLATES

Since an ideal template would be one layer of spheres thick, we assessed thickness as a function of spinning speed for templates prepared from silica suspension in acetone. AFM height profiles were obtained across a radially drawn scratch (Figure 4.16A) at several distances from the spinning center. Figure 4.16B shows one such line scan. The average height of the deposit was calculated, equal to the difference between the zero level and the average

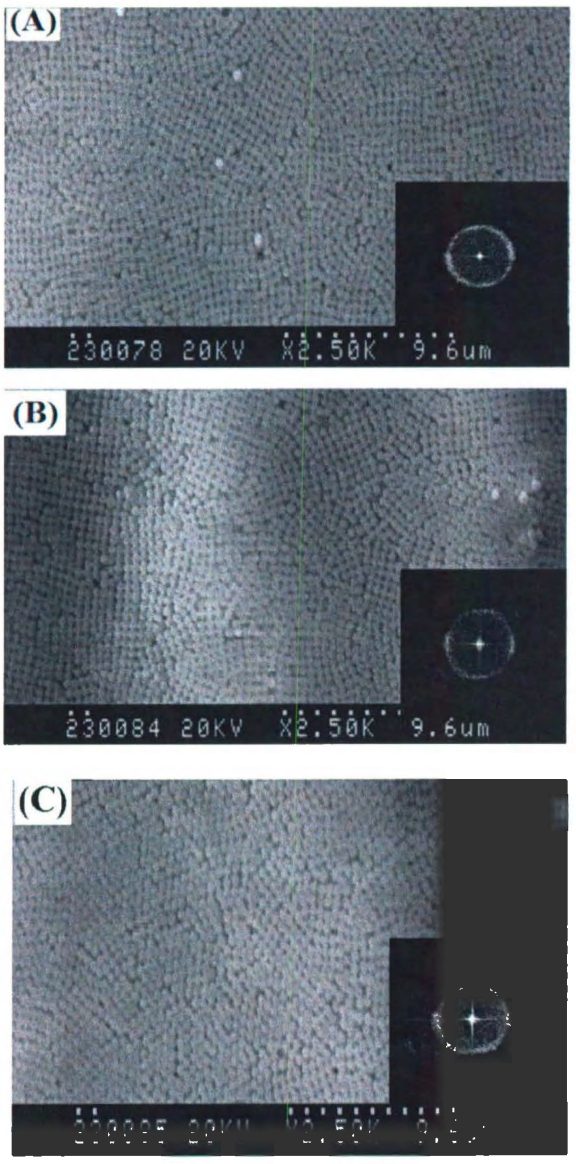

Figure 4.15: Scanning electron micrographs of 3 regions (and their FFTs, insets) for a sample prepared at 7000 rpm by spin coating an acetone suspension. (A) [100]-oriented packing is observed 2 mm from the spinning center. The FFT is diffuse because there is poor order close to the center. (B) At 5 mm from the spinning center, [100]-oriented packing is observed. There is a hint of four-fold symmetry in the FFT. (C) There is no sign of four-fold symmetry, but clear signs of six-fold symmetry at a distance of 6 mm from the center of spinning.

colloidal deposit level. The hump near the edge of the scratch may be the result of colloidal residue. The samples were annealed at 300° C before scratching. This reduces the scratching of sample by the AFM tip. Heights were measured for samples prepared by spin coating acetone colloidal suspension at speeds of 3000 - 8000 rpm. Colloidal crystal thickness decreases as the speed of rotation increases (Figure 4.17). All samples whose data are shown here are between 2 and 4 layers thick. (Dotted and dashed lines show integer layer numbers for "square" (fcc (100), face is parallel to substrate) and "hexagonal" (fcc (111), face parallel to substrate) structures respectively.) Our results are consistent with a power law (Section 2.1) $H = \omega^{-(0.43 \pm 0.06)}$ (Figure 4.17, Inset). Within error, the power law exponent is in the range of values 0.44 - 0.51 obtained by Rehg *et al.*[37] for salt concentrations ranging from 0.0 - 0.1 M.

Colloidal films with thicknesses less than one full layer could possibly correspond to regions with mixed symmetries. There is four-fold symmetry up to 5500 rpm (Figure 4.2A: Four-fold-1), with corresponding thicknesses of at least three complete particle layers. The transition region in Figure 4.3A (six-fold and mixed) appears to occur only for samples with thickness between two and three layers.

4.6 UNIFORMITY AND LATERAL PERIODICITY IN TEMPLATED COBALT SAMPLES

Cobalt was electrodeposited through spin coated templates and then the colloids were etched away by hydrofluoric acid to leave a patterned cobalt material (discussed in Chapter 3). The shape, crystalline phase, and thickness of a templated electrodeposit plays an important role in tuning its magnetic properties.[30,32,50] Thus, it is important to analyze the lateral periodicity and the thickness uniformity of a templated samples. The overall scheme developed

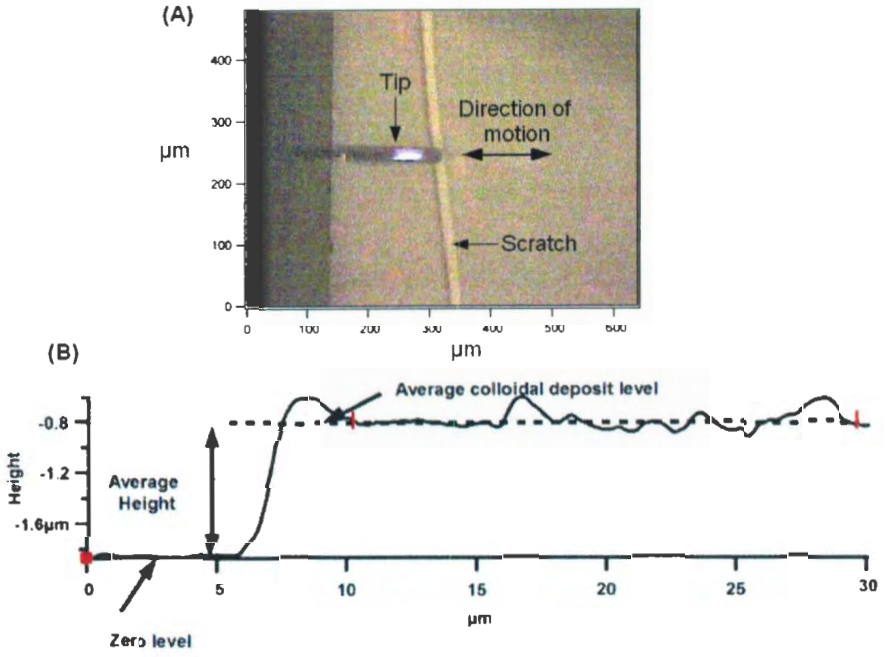

Figure 4.16: (A) A view of a scratched colloidal template from the camera mounted on the AFM. The tip moves across the scratch to give height profiles like that shown in (B). The zero level is the bare substrate (in the scratch) and the average level represents the average height of the colloidal deposit.

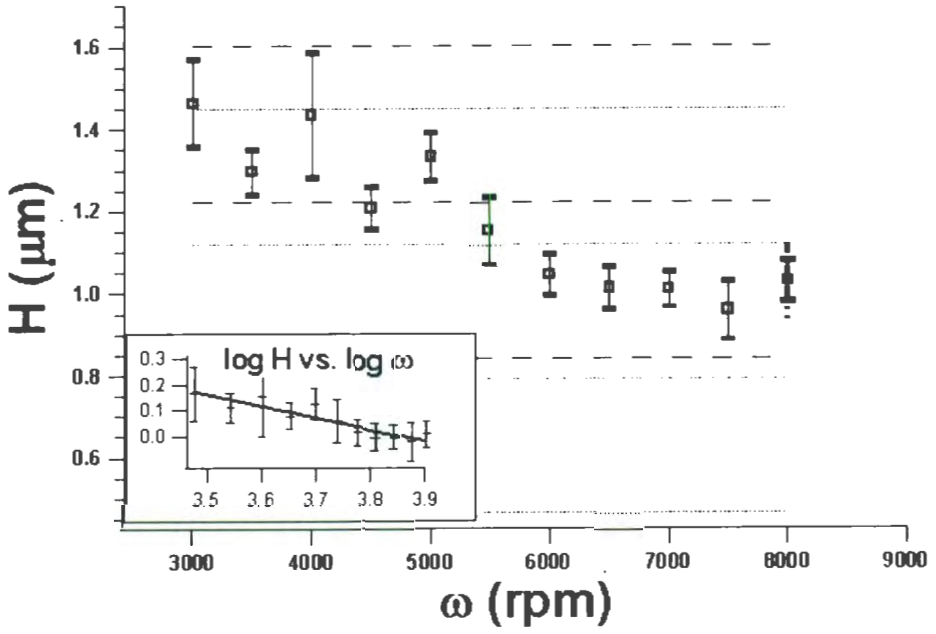

Figure 4.17: (a) Templates prepared by evaporative spin coating at different angular velocities ω have different thicknesses. Thickness H (the average height of colloid surface) *vs.* ω shows template thicknesses between 2 and 4 layers. Solid and dashed lines are the expected thicknesses for integer number (1 to 4) of "square" (fcc (100), face parallel to substrate) and "hexagonal" (fcc (111), face parallel to substrate) packing orientations. A fit to a ω^{-N} power law (inset) yields $N = 0.43 \pm 0.06$, consistent with the values (0.44-0.51 for 0.0 - 0.1M salt concentrations) obtained by Rehg *et al.*[37]

during this thesis work is shown in Figure 4.18.

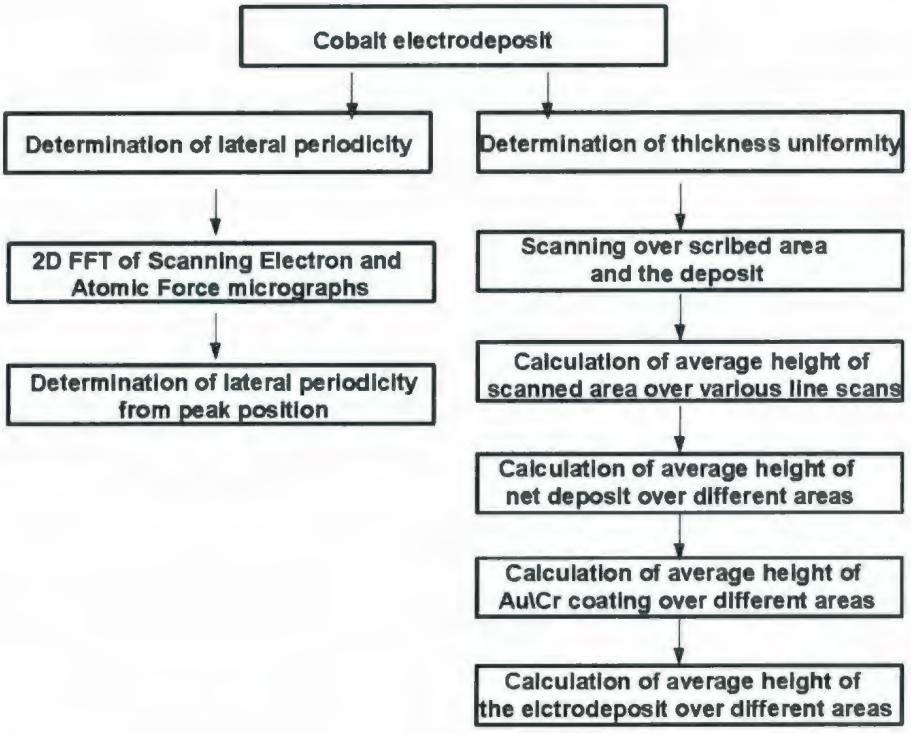

Figure 4.18: The overall scheme for determining uniformity and lateral periodicity in our electrodeposited samples.

4.6.1 DETERMINATION OF LATERAL PERIODICITY

One can determine the lateral periodicity present in a sample from the FFT of its SEM images. One expects the appearance of peaks if long range ordering of pores is present in the sample or a bright circular ring if the long range order is absent. Figure 4.19A shows a scanning electron micrograph of a region in the patterned cobalt sample, and its corresponding 2D FFT is given in Figure 4.19C. (This sample was prepared by electrodepositing cobalt at -1.2 V *vs.* Ag/AgCl, from 0.1 M $CoSO_4$ and 0.1 M H_3BO_3, through a spin coated template

(prepared by spin coating a silica suspension in acetone at 3000 rpm), followed by HF etching in 1% HF for 2 minutes). The bright regions in the SEM image correspond to the cobalt deposit and the dark regions are voids left after removing the colloidal spheres. The presence of four peaks in the FFT shows that the electrodeposit has four-fold symmetry. We used a software (ImageJ) to produce FFT of an image and calculate the lateral periodicity present in the sample. The generated FFT of the image is unscaled (the distance from center to a peak distance in a FFT (q_u) is in unscaled reciprocal-space pixels). The lateral periodicity (p) (present in the imaged region, Figure 4.19A) can be calculated by measuring center to peak distance (q_u) in the FFT (Figure 4.19C), and by using the equation

$$p = \left(\frac{1024}{q_u} \times \frac{4.8}{191} \right) \mu m, \tag{4.1}$$

for a 1024 × 1024 pixel FFT image. The scale is set by measuring the length of the SEM image scale bar (4.8 μm / 191 pixels). The average value of lateral periodicity (for four peaks in a FFT) for the SEM image shown in Figure 4.19A is 0.50 ± 0.01 μm, which is equal to the diameter of the removed colloidal spheres and is an expected result. This shows that the colloidal spheres in the template are not being pushed during electrodeposition of cobalt.

One would also expect to see four-fold symmetry in the FFT of AFM images in the same region of the same sample. Figure 4.19B shows an AFM image of a similar area in the same sample as in Figure 4.19A. One can see by eye the presence of the four-fold symmetry in the image, but the FFT of the image, showing four peaks is more convincing (Figure 4.19D). The lateral periodicity from AFM images was calculated by the same procedure used for SEM images. The calculated value of lateral periodicity for the AFM image shown in Figure 4.19B is 0.51 ± 0.02 μm, which is equal to the diameter of removed silica spheres and is an expected result.

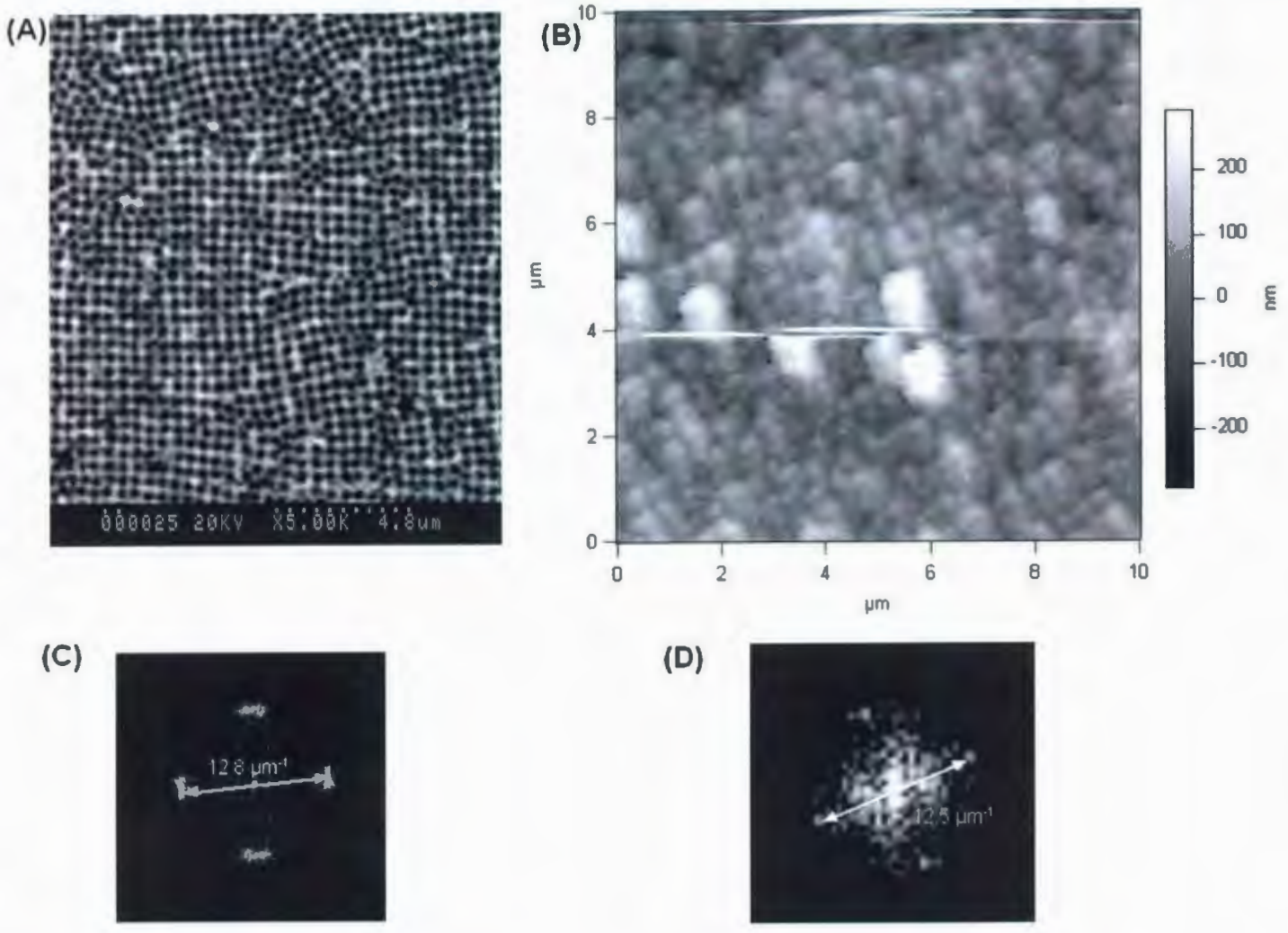

Figure 4.19: (A) A scanning electron micrograph of a patterned cobalt sample. (B) An AFM image of a similar area in the same sample. FFTs of the SEM (C) and AFM (D) images consist of four peaks, indicating the presence of four-fold symmetry.

4.6.2 DETERMINATION OF THICKNESS UNIFORMITY

In order to calculate thickness of the deposit using AFM, one needs to scan over an edge of the deposit as we did for the template (Section 4.5), scribing the sample with a blade to get a sharp edge. Figure 4.20B shows a representative line scan over a scribed edge. Assuming the zero height level corresponds to the top surface of the glass coverslip, the height at the top of the deposit will be the height of the electrodeposit in addition to the gold and chromium layers. The thickness of chromium and gold deposits can be determined in the same way, by scanning over a scratch in a region without a cobalt electrodeposit, and this height can be subtracted to get the height of the electrodeposit. We assume that the glass is uniformly coated with gold and chromium.

The uniformity in the thickness along the sample can be calculated by averaging the height calculated from several or successive line scans in the same area, and then comparing results at different places on the sample. In this thesis work, we neglected the edges of the deposit because they look much thicker than the rest of the deposit. Our scheme works well on an untemplated cobalt electrodeposit on Au/Cr/glass. Figure 4.20A shows a representative AFM image. Several sets of consecutive line scans (such as the one shown in the Figure 4.20B) in horizontal direction were chosen to calculate the average height of this area. For the area scan shown in Figure 4.20A, this average height is 61 $\pm$ 14 nm, based 2 sets of 11 line scans, spaced 5 μm apart. The standard deviation is associated with the variation in the average height of a single line scan. This procedure was repeated on two more area scans, each separated by 0.5 mm. The average height over this 1 mm of the sample was 60 $\pm$ 17 nm. Our procedure could be used in future studies to calculate the thickness uniformity of patterned cobalt samples.

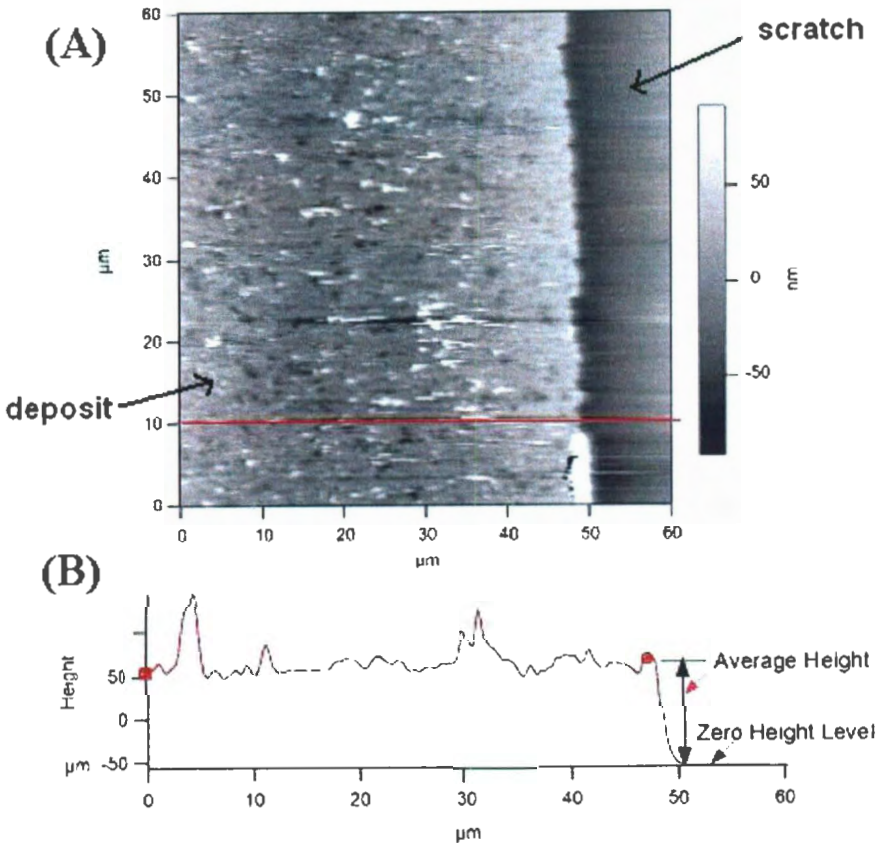

Figure 4.20: (A) A representative AFM image of electrodeposited cobalt on Au/Cr/glass and a corresponding line scan (B). The zero level in (B) corresponds to the glass and the average height corresponds to the average height of the Co/Au/Cr.

Chapter 5

CONCLUSIONS

The work in this thesis is focused on the preparation of cobalt patterns by electrodeposition through colloidal templates prepared by spin coating. Much of the work is concentrated on elucidating the structure of colloidal templates prepared by spin coating and optimizing the preparation technique for synthesizing visually uniform patterned cobalt samples. A scheme is designed to quantify the lateral periodicity present in the cobalt array and uniformity in the height of a sample.

The structure of the template was studied using a real-space technique (scanning electron microscopy) and reciprocal-space techniques (laser diffraction and white light diffraction). The templates were prepared by varying two parameters, *i.e.* spin coating solvent and spin speed. Both spin coating solvent and the spin speed have an influence on the symmetry present in the structure of the spin coated colloidal sample. A star-like reflection was observed when samples were viewed at an oblique angle. We conclude that at lower speeds (3000-5500 rpm), the samples prepared by spin coating the colloidal suspension in acetone consist of small domains ($\sim 10\ \mu$m) with [100]-oriented fcc structure, whereas at same speeds the samples prepared by spin coating the colloidal suspension in ethanol consist of domains with [111]-oriented fcc structure. A six-fold reflection, and [111]-oriented fcc domains

were observed for the sample prepared at 6000 rpm, which changes into four-fold reflection, and [100]-oriented fcc domains at 8000 rpm with the wide transition from 6500-7500 rpm. The transition region consist of samples with mixed symmetries, 4-fold near to the center ([100]-oriented fcc domain structure) followed by six-fold symmetric region ([100]-oriented fcc domain structure). In the case of ethanol, the four-fold symmetric sample was observed only at a spin speed of 8000 rpm, with no wide transition region. The study of dynamics underlying the transition is relatively untouched. We have varied only two parameters, while there are many factors like humidity, temperature, vapor pressure, roughness of substrate and viscosity that can be varied to fully understand the process of spin coating.

SEM studies showed that all samples are polycrystalline and consist of domains oriented in different directions. The FFT of scanning electron micrographs coupled with the laser diffraction data revealed that the domains are correlated such that there exists an average direction of periodicity over a mm-scale region. The mm-scale polycrystalline regions are further orientationally correlated, and are arranged in "circular"- manner to give rise to a visual symmetry (star-pattern) on the sample. We call this crystal an Orientationally Correlated Polycrystal (OCP) because it has long-range order in spite of being polycrystalline and having only short-range translational periodicity. The orientational correlation was quantified by studying the angular correlations between laser diffraction patterns obtained at different positions on a sample. The cross-correlation demonstrates the progressive rotation of the OCP region with off-center translation. Along the radial direction the orientation of the OCP region stays the same. The autocorrelation function was calculated to measure domain orientational dispersion in the laser diffraction peaks. The value of domain orientational dispersion decreased from 27° at the center to $\approx 13°$ for the distances greater than 2 mm.

The preparation of patterned cobalt by electrodeposition through colloidal templates is a multi-step procedure. Aiming to electrodeposit visually uniform cobalt from $CoSO_4$, various parameters involved at each step of the synthesis are varied. We conclude that annealing

at 300 °C is required for stabilizing the templates during electrodeposition. A weak buffer (H_3BO_3) is required to stabilize the electrolyte's pH, and thus, to improve the quality of the electrodeposit. The deposition is highly sensitive to the method used for cleaning the substrates prior to spin coating. Cleaning of substrates with acetone vapors and fresh H_2SO_4 were found to be the two most promising cleaning methods, but visually uniform deposits were obtained randomly with these cleaning techniques. Even though lots of combinations and procedures were tested for each step, a reliable procedure to make a uniform cobalt deposit is still not clear and require further studies. The time for etching silica using HF is not optimized because of non-uniformity of the cobalt electrodeposit.

A scheme for quantifying the lateral periodicity present in a patterned cobalt was devised using atomic force micrographs and scanning electronic micrographs of the sample surface. Better AFM scans are required for this analysis. The thickness of the electrodeposit was measured by scanning the sample using AFM and a scheme was designed using untemplated cobalt electrodeposit on Au/Cr/glass. The scheme needs to be applied to the templated samples to find the order of uniformity. This analysis requires a uniform templated cobalt sample. Once the average height of a uniform sample is calculated using AFM, one can optimize the electrodeposition parameters to get a cobalt pattern of specific thickness and can also optimize the time for etching the colloids in future.

While writing the manuscript, a very relevant work by Vermolen *et al.*[51] came to our attention, with results very similar to the work described in this thesis, and providing confirmation of the summary of our work published in Physical Review E.[21] Vermolen[51] points out that the crystallization in evaporative spin coating is driven by three fluid flows *i.e.* radial, tangential and vertical. Identifying the relative contributions of the different flows could be an interesting future project. Another possibility for a future project is an extensive study of the effect of substrate type and of substrate cleaning on electrodeposition of a material though colloidal template.

Appendix A

SYNTHESIS AND CHARACTERIZATION OF SILICA COLLOIDS

This section describes the synthesis and characterization of spherical colloidal silica particles. The synthesis was done by Stöber's method[52] and using Giesche conditions.[53 55] The basic two step reaction involved in the synthesis of silica colloidal particles is described below:

$$Si(OC_2H_5)_4 + 4H_2O \xrightarrow[\text{ethanol}]{NH_3} Si(OH)_4 + 4C_2H_5OH \tag{A.1}$$

$$Si(OH)_4 \xrightarrow[\text{ethanol}]{NH_3} SiO_2 \downarrow + 2H_2O \tag{A.2}$$

Anhydrous ethyl alcohol (Commercial Alcohols Inc., bp 78°C), TEOS (Fluka, purum, $\geq$ 98.0%, bp 168°C) was freshly distilled before use[55] for the synthesis of spherical particles. The scanning electron micrographs of the resulting air-dried silica particles is shown in Figure A.1. The silica colloidal particles have more than 6% polydispersity. Because of this high polydispersity, these silica particles did not form crystals during spin coating of

their suspensions in acetone. A mixture of synthesized and commercially available silica particles (Fiber Optic Center, SIO2P050-1 microspheres of diameter 458nm ± 2 nm with low size polydispersity, since no calibration standard was used, possible systematic errors in particle diameter is 5 %) did not form a crystalline stucture during spin coating either. Diameter were measured *via* SEM from center-to-center distance of 10 spheres along a line in a hexagonal layer of air-dried spheres, and from laser diffraction data from similar colloidal templates prepared by spin coating a colloidal suspension in acetone. Thus, for the thesis work, colloidal template were prepared only from commercially available silica particles.

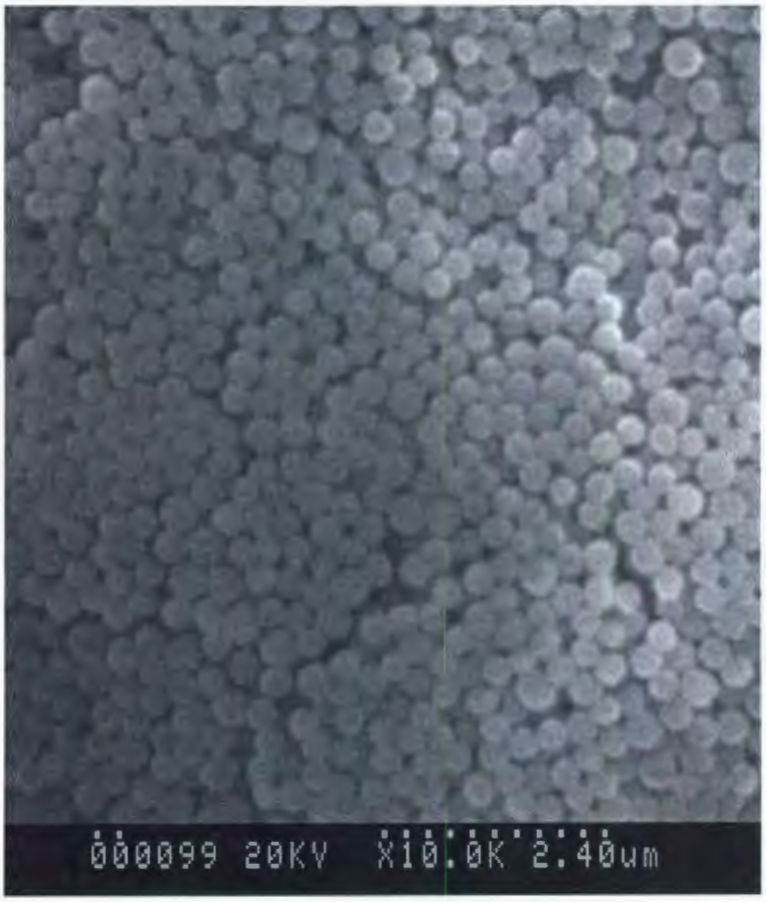

Figure A.1: The scanning electron micrographs of the silica particles produced by Stöber's method. The size polydispersity is more than 6 %.

Appendix B

SAMPLE PREPARATION

Coating composition$_1$	*Substrate cleaning*$_{1-4}$	*Colloid solvent*	*Annealing* 5,6	*Template cleaning*$_1$	*Electrolyte* 7,8	*Remarks* 9–12
Thick-Au/Cr	H_2SO_4/H_2O**	None	-	H_2O	0.01 M (C/B)	NU
Thick-Au/Cr	H_2SO_4*/H_2O	None	-	H_2O	0.01 M (C/B)	U/R
Thick-Au/Cr	H_2SO_4/H_2O	None	-	H_2O	0.01 M (C/B)	U
Thick-Au/Cr	Ethanol	None	-	-	0.01 M (C/B)	NU (patches)
Thick-Au/Cr	Ethanol(S)	None	-	H_2O	0.01 M (C/B)	NU (patches)
Thick-Au/Cr	Acetone	None	-	H_2O	0.01 M (C/B)	U
Thick-Au/Cr	Acetone (S)	None	-	H_2O	0.01 M (C/B)	NU (patches)
Thick-Au/Cr	Acetone (V)	None	-	H_2O	0.01 M (C/B)	U
Thick-Au/Cr	$H_2SO_4{}^{2min}/H_2O$	None	-	-	-	P

Continued on next page

Coating composition[1]	*Substrate cleaning*[1–4]	*Colloid solvent*	*Annealing* [5,6]	*Template cleaning*[1]	*Electrolyte* [7,8]	*Remarks* [9–12]
Thick-Au/Cr	$H_2SO_4{}^{3min}/H_2O$	None	-	-	-	P
Thick-Au/Cr	$H_2SO_4{}^{5min}/H_2O$	None	-	-	-	P
Thick-Au/Cr	H_2SO_4/H_2O	acetone	300° C (A)	H_2O	0.01 M (C/B)	U (randomly)
Thick-Au/Cr	Acetone (V)	acetone	300° C (A)	H_2O	0.01 M (C/B)	U
Thin-Au/Cr	H_2SO_4*/H_2O	acetone	300° C (A)	H_2O	0.01 M (C/B)	P
Thin-Au/Cr*	H_2SO_4*/H_2O**	acetone	300° C (A)	H_2O	0.01 M (C/B)	NU (patches)
Thin-Au/Cr*	H_2SO_4*/H_2O	acetone	300° C (A)	-	0.01 M (C/B)	NU (patches)
Thin-Au/Cr*	H_2SO_4*/H_2O	acetone	300° C (A)	H_2O	0.01 M (C/B)	NU (patches)
Thin-Au/Cr*	H_2SO_4*/H_2O	acetone	300° C (A)	H_2SO_4*/H_2O	0.01 M (C/B)	NU (patches)
Thin-Au*	H_2SO_4*/H_2O**	acetone	300° C (D)	H_2O	0.1 M (C)	U
Thin-Au	H_2SO_4*/H_2O	acetone	400° C (D)	H_2O	0.1 M (C)	P
Thin-Au	H_2SO_4*/H_2O	acetone	500° C (D)	H_2O	0.1 M (C)	P
Thin-Au	H_2SO_4*/H_2O	acetone	600° C (D)	Sample melts	-	-
Thin-Au*	H_2SO_4*/H_2O	acetone	300° C (A)	H_2O	0.01 M (C/B)	U/R

Table B.1: Preparation conditions explored for synthesizing templates and patterned cobalt samples. Further details are given in Chapter 3.

[1]*: Not Fresh (Substrates: Prepared few months back, H_2SO_4: used for general cleaning in our lab
[2]**: substrate glued on microscope slide during cleaning procedure
[3]S: From suspension
[4]V: Acetone vapors
[5]A: Annealing with ramp up (100° C/hr) + dwell (3 hours)
[6]D: Annealing with ramp up (100° C/hr) + dwell (3 hours) + ramp down to 50° C(100° C/hr)
[7]C: $CoSO_4$
[8]B: H_3BO_3
[9]NU: Visually non-uniform
[10]P: Gold substrate layer peeling
[11]R: Non-uniform at the places with residue left during cleaning.
[12]U: Visually uniform

Appendix C

ADDITIONAL LASER DIFFRACTION PATTERNS

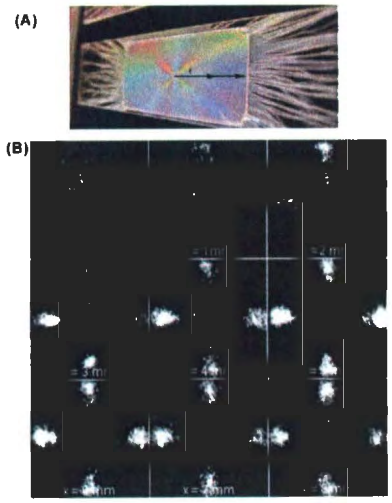

Figure C.1: Upon translation along the radial direction shown in (A), nine successive laser diffraction patterns were obtained (B). These diffraction data correspond to $y = 0$ mm, obtained at 1 mm intervals from $x = 0$ mm to $x = 8$ mm. The sample was spin coated at 3000 rpm from a silica suspension in acetone.

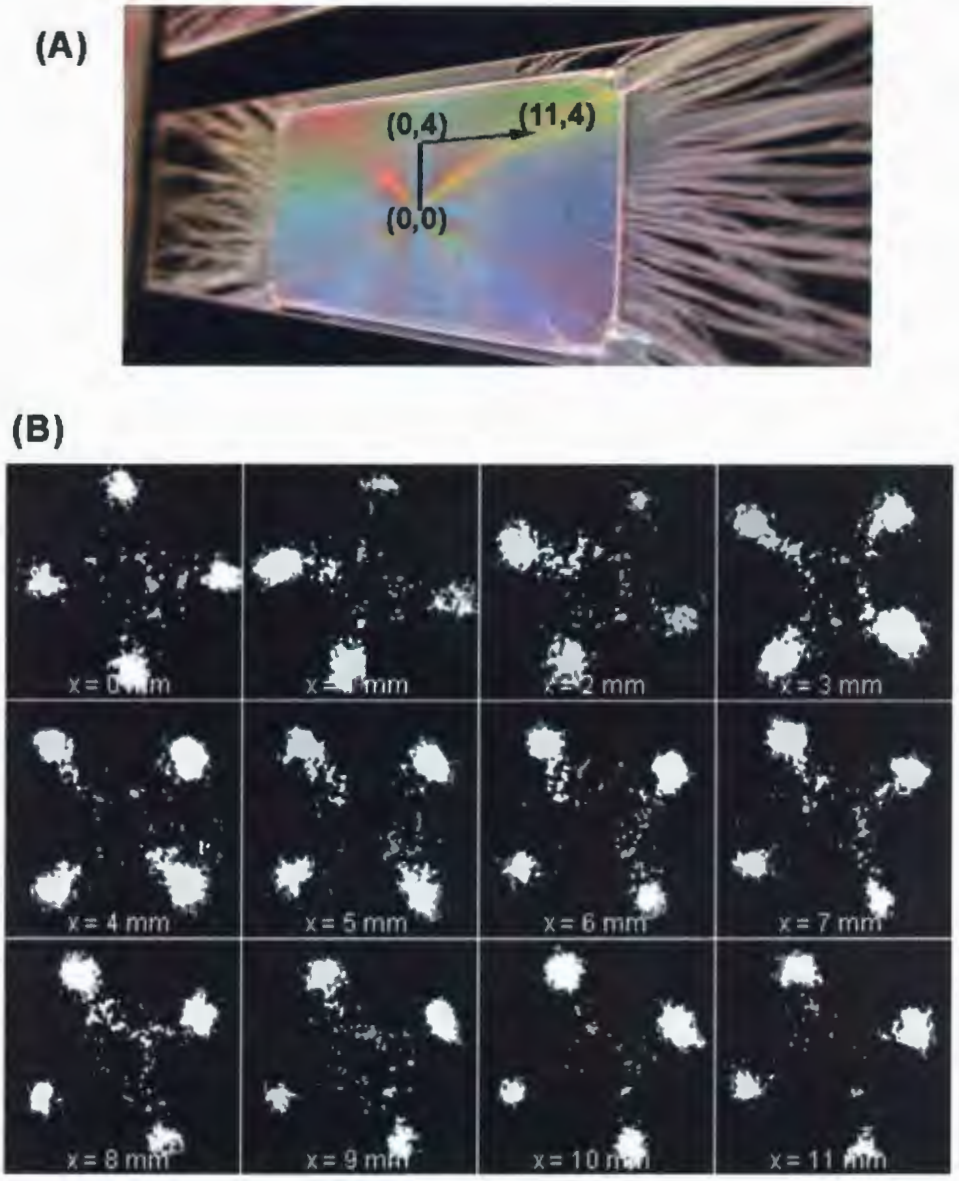

Figure C.2: Upon translation along the off-center direction shown in (A), twelve successive laser diffraction patterns were obtained (B). These diffraction data correspond to $y = 4$ mm, obtained at 1 mm intervals while moving outward in the sample (off-center) in a straight line. The sample was spin coated at 3000 rpm from a silica suspension in acetone.

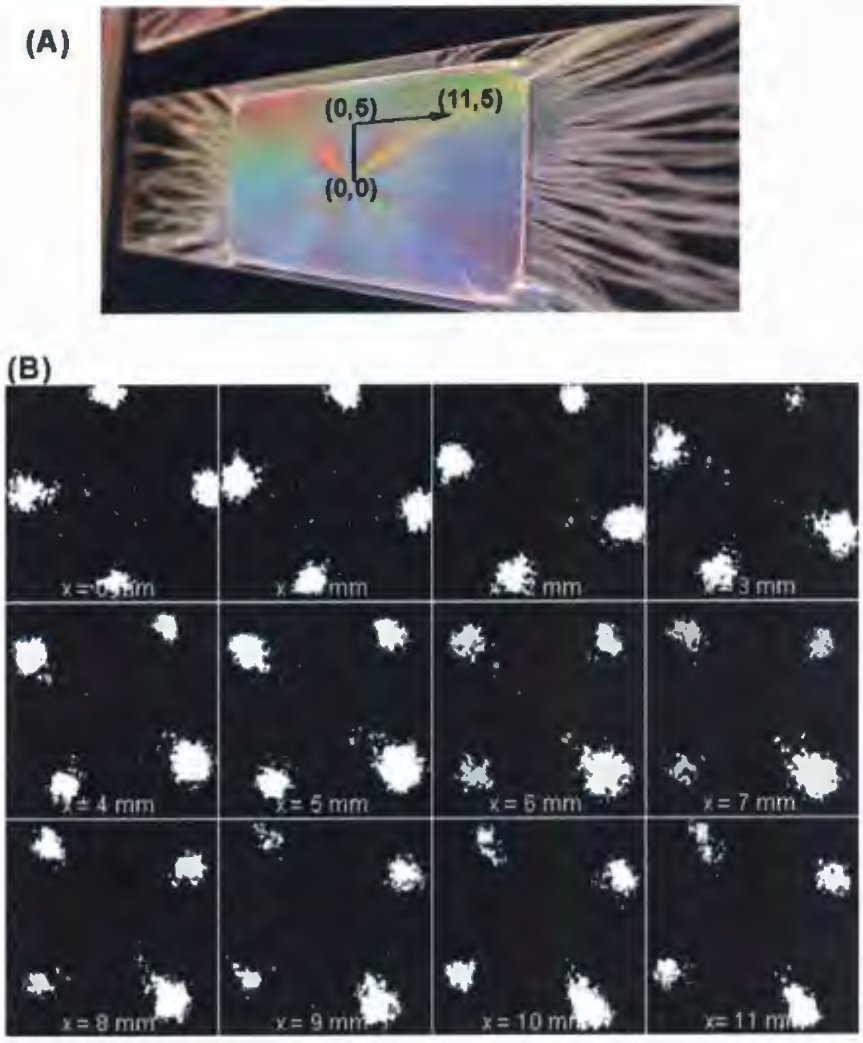

Figure C.3: Upon translation along the off-center direction shown in (A), twelve successive laser diffraction patterns were obtained (B). These diffraction data correspond to $y = 5$ mm, obtained at 1 mm intervals while moving outward in the sample (off-center) in a straight line. The sample was spin coated at 3000 rpm from a silica suspension in acetone.

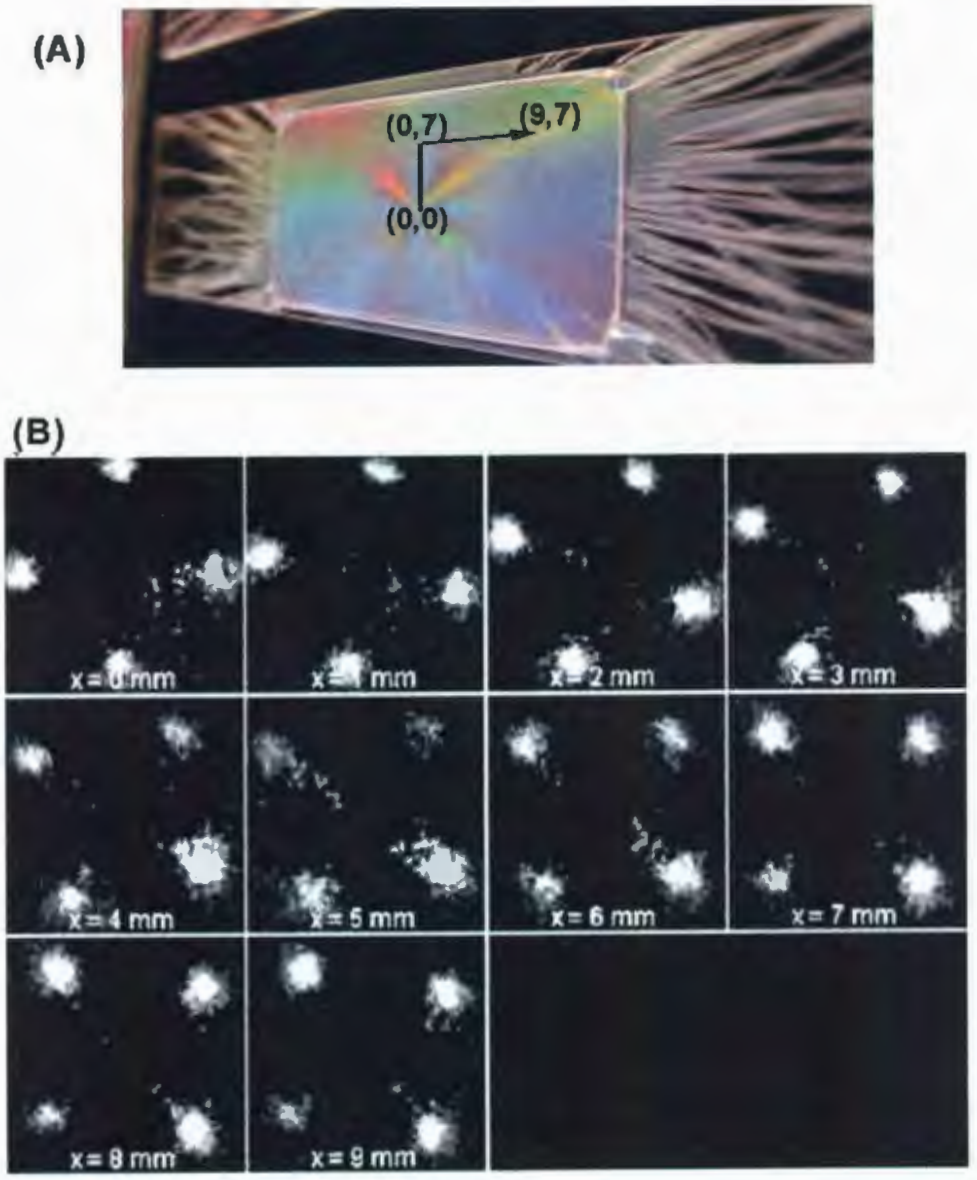

Figure C.4: Upon translation along the off-center direction shown in (A), ten successive laser diffraction patterns were obtained (B). These diffraction data correspond to $y = 7$ mm, obtained at 1 mm intervals while moving outward in the sample (off-center) in a straight line. The sample was spin coated at 3000 rpm from a silica suspension in acetone.

Bibliography

[1] J.W. Goodwin. *Colloids and Interfaces with Surfactants and Polymers.* John Wiley and Sons, 2004.

[2] D.J. Norris, E.G. Arlinghaus, L. Meng, R. Heiny, and L.E. Scriven. Opaline photonic crystals: How does self-assembly work? *Advanced Materials*, 16:1393 1399, 2004.

[3] J.H. Holtz and S.A. Asher. Polymerized colloidal crystal hydrogel films as intelligent chemical sensing materials. *Nature*, 389:829 832, 1997.

[4] C.M. Cornelius and J.P. Dowling. Modification of Planck blackbody radiation by photonic band-gap structures. *Physical Review A*, 59:4736 4746, 1999.

[5] S.Y. Lin, J.G. Fleming, E. Chow, J. Bur, K.K. Choi, and A. Goldberg. Enhancement and suppression of thermal emission by a three-dimensional photonic crystal. *Physical Review B*, 62:2243 2246, 2000.

[6] J.G. Fleming, S. Y. Lin, E. Kady, R. Biswas, and K.M. Ho. All-metallic three-dimensional photonic crystals with a large infrared bandgap. *Nature*, 417:52 55, 2002.

[7] J.M. Weissman. Thermally switchable periodicities and diffraction from mesoscopically ordered materials. *Science*, 274:959 963, 1996.

[8] Y. Xia. Self-assembly approaches to three-dimensional photonic crystals. *Advanced Materials*, 12:693 713, 2000.

[9] R.M. Amos, J.G. Rarity, P.R. Tapster, and T.J. Shepherd. Fabrication of large-area face-centered-cubic hard-sphere colloidal crystals by shear alignment. *Physical Review E*, 61:2929 2935, 2000.

[10] O. Vickreva, O. Kalinina, and E. Kumacheva. Colloid crystal growth under oscillatory shear. *Advanced Materials*, 12:110 112, 2000.

[11] J.P. Hoogenboom, P. Vergeer, and A. van Blaaderen. A real-space analysis of colloidal crystallization in a gravitational field at a flat bottom wall. *Journal of Chemical Physics.*, 119:3371 3383, 2003.

[12] A. Yethiraj, J.H.J. Thijssen, A. Wouterse, and A. van Blaaderen. Large-area electric-field-induced colloidal single crystals for photonic applications. *Advanced Materials*, 16:596 600, 2004.

[13] M. Trau, D.A. Saville, and I.A. Aksay. Assembly of colloidal crystals at electrode interfaces. *Langmuir*, 13:6375 6381, 1997.

[14] M. Yoldi, W. González-Viñas, M.C. Arcos, and R. Sirera. Electrophoretic deposition of colloidal crystals assisted by hydrodynamic flows. *Journal of Materials Science*, 41:2965 2969, 2006.

[15] P. Maraghechi and A.Y. Elezzabi. The design of a reversible wafer holder for uniform photoresist coatings of deeply etched cavities. *Measurement Science and Technology*, 19:1 5, 2008.

[16] B. Menaa, M. Takahashia, Y. Tokudaa, and T. Yoko. High optical quality spin-coated polyphenylsiloxane glass thick films on polyethyleneterephtalate and silica substrates. *Materials Research Bulletin*, 41:1925 1934, 2006.

[17] I.M. Thomas. High laser damage threshold porous silica antireflective coating. *Applied Optics*, 25:1481 1483, 1986.

[18] P. Jiang and M.J. McFarland. Large-scale fabrication of wafer-size colloidal crystals, macroporous polymers and nanocomposites by spin-coating. *Journal of the American Chemical Society*, 126:13778 13786, 2004.

[19] A. Mihi, M. Ocana, and H. Miguez. Oriented colloidal-crystal thin films by spin-coating microspheres dispersed in volatile media. *Advanced Materials*, 18:2244 2249, 2006.

[20] T. Ogi, L.B. Modesto-Lopez, F. Iskandar, and K. Okuyama. Fabrication of a large area monolayer of silica particles on a sapphire substrate by a spin coating method. *Colloids and Surfaces A: Physicochemical Engineering Aspects*, 297:71 78, 2007.

[21] C. Arcos, K. Kumar, W. González-Viñas, R. Sirera, K.M. Poduska, and A.Yethiraj. Orientationally correlated colloidal polycrystals without long-range positional order. *Physical Review E*, 77:050402/1 4, 2008.

[22] S.H. Charap, P. Lu, and Y. He. Thermal stability of recorded information at high densities. *IEEE Transactions on Magnetics*, 15:373 382, 2001.

[23] C.A. Ross. Patterned magnetic recording media. *Annual Review of Materials Research*, 31:203 235, 2001.

[24] S.Y. Chou. Patterned magnetic nanostructures and quantized magnetic disks. *Proceedings of the IEEE*, 85:652 671, 1997.

[25] J.-P. Wang, J.-M. Qiu, T. A. Taton, and B.-S. Kim. Direct preparation of highly ordered $L1_0$ phase FePt nanoparticles and their shape-assisted assembly. *IEEE Transactions on Magnetics*, 42:3042 3047, 2006.

[26] Y. Peng W. Li, J. Zhang, G.A. Jones, and T.H. Shen. Magnetic and magneto optical characteristics of nanowire arrays embedded in anodic aluminium oxide. *Journal of Physics Conference Series*, 17:20 32, 2005.

[27] D. Pullinia, D. Busquets, A. Ruotolo, G. Innocenti, and V. Amigo. Insights into pulsed electrodeposition of GMR multilayered nanowires. *Journal of Magnetism and Magnetic Materials*, 316:242 245, 2007.

[28] O. Seifarth, I. Tokarev R. Krenek, Y. Burkov, A. Sidorenko, and D. Schmeiber, S. Minko, M. Stamm. Metallic nickel nanorod arrays embedded into ordered block copolymer templates. *Thin Solid Films*, 515:6552 6556, 2007.

[29] J.C. Kim, Y.N. Kim, N.H. Hur, W.S. Kim, and Y.G. Kang. Highly ordered macroporous magnetic materials prepared by electrodeposition through colloidal template. *Physica Status Solidi (b)*, 241:1585 1588, 2004.

[30] A.A. Zhukov, M.E. Kiziroglou, A.V. Goncharov, R. Boardman, M.A. Ghanem, M. Abdelsalam, V. Novosad, G. Karapetrov, H. Fangohr X. Li, C. H. de Groot, P. N. Bartlett, and P. A. J. de Groot. Shape-induced anisotropy in antidot arrays from self-assembled templates. *IEEE Transactions on Magnetics*, 41:3598 3600, 2005.

[31] P.N. Bartlett, M.A. Ghanem, I.S. El Hallag, P. de Groot, and A. Zhukov. Shape-induced anisotropy in antidot arrays from self-assembled templates. *Journal of Materials Chemistry*, 13:2596 2602, 2003.

[32] A.K. Srivastava, S. Madhavi, T.J. White, and R.V. Ramanujan. Template assisted assembly of cobalt nanobowl arrays. *Journal of Materials Chemistry*, 15:4424 4428, 2005.

[33] W. Liu, W. Zhong, L.J. Qiu, L.Y. Lu, and Y.W. Du. Fabrication and magnetic behaviour of 2D ordered Fe/SiO_2 nanodots array. *The European Physical Journal B*, 51:501 506, 2006.

[34] R.M. Bozorth. Magnetism. *Reviews of Modern Physics*, 19:29 86, 1947.

[35] N.A. Spaldin. *Magnetic Materials: Fundamentals and Device Applications*. Cambridge University Press, 2003.

[36] B.D Washo. Rheology and modeling of the spin coating process. *IBM Journal Of Research and Development*, 21:190 198, 1977.

[37] T.J. Rehg and B.G. Higgins. Spin coating of colloidal suspensions. *American Institute of Chemical Engineers Journal*, 38:489 501, 1992.

[38] D.E. Bornside, C.W. Macosko, and L.E. Scriven. On the modeling of spin coating. *Journal of imaging technology*, 13:122 130, 1987.

[39] A.G. Emslie, F.T. Bonner, and L.G. Peck. Flow of a viscous liquid on a rotating disk. *Journal of Applied Physics*, 29:858 862, 1958.

[40] T. Ogi, L.B. Modesto-Lopez, F. Iskandar, and K. Okuyama. Fabrication of a large area monolayer of silica particles on a sapphire substrate by a spin coating method. *Colloids and Surfaces A: Physicochemical and Engineering Aspects*, 297:71 78, 2007.

[41] C.G. Zoski. *Handbook of Electrochemistry*. Elsevier, 2007.

[42] J.W. Dini. *Electrodeposition*. William Andrew Inc., 1993.

[43] A.J. Bard and L.R. Faulkner. *Electrochemical methods: fundamentals and applications*. John Wiley and Sons Inc, 2000.

[44] S. Lee and L. Lee. *Encyclopedia of chemical processing*. CRC Press, 2005.

[45] J. Goldstein, P. Echlin D.E. Newbury, D.C. Joy C.E. Lyman, E. Lifshin, L.C. Sawyer, and J.R. Michael. *Scanning Electron Microscopy and X-ray Microanalysis*. Springer, 2003.

[46] L. Reimer. *Scanning Electron Microscopy: Physics of Image Formation and Microanalysis*. Springer, 1998.

[47] V.J. Morris, A.R. Kirby, and A.P. Gunning. *Atomic Force Microscopy for Biologists*. Imperial College Press, 1999.

[48] E. Meyer, H.J. Hug, and R. Bennewitz. *Scanning Probe Microscopy*. Springer, 2004.

[49] H. Miguez, S.M. Yang, N. Tetreault, and G.A. Ozin. Oriented free-standing three-dimensional silicon inverted colloidal photonic crystal microfibers. *Advanced Materials*, 14:1805 1808, 2002.

[50] W. Sucksmith and J.E. Thompson. The magnetic anisotropy of cobalt. *Proceedings of the Royal Society of London- Series A*, 225:362 375, 1954.

[51] Esther Vermolen. Manipulation of colloidal crystallization. Master's thesis, Utrecht University, November 2008.

[52] W. Stöber, A. Fink, and E. Bohn. Controlled growth of monodisperse silica spheres in micron size range. *Journal of Colloid Interface Science*, 26:62 69, 1968.

[53] H. Giesche. Synthesis of monodispersed silica powders i: particle properties and reaction kinetics. *Journal of European Ceramic Society*, 14:189 204, 1994.

[54] H. Giesche. Synthesis of monodispersed silica powders ii: controlled growth reactions and continuous production processes. *Journal of European Ceramic Society*, 14:205 214, 1994.

[55] N. Li. Colloidal ordering under external electric fields. Master's thesis, Memorial University, May 2008.